

RAF1 amplification drives a subset of bladder tumors and confers sensitivity to MAPK-directed therapeutics

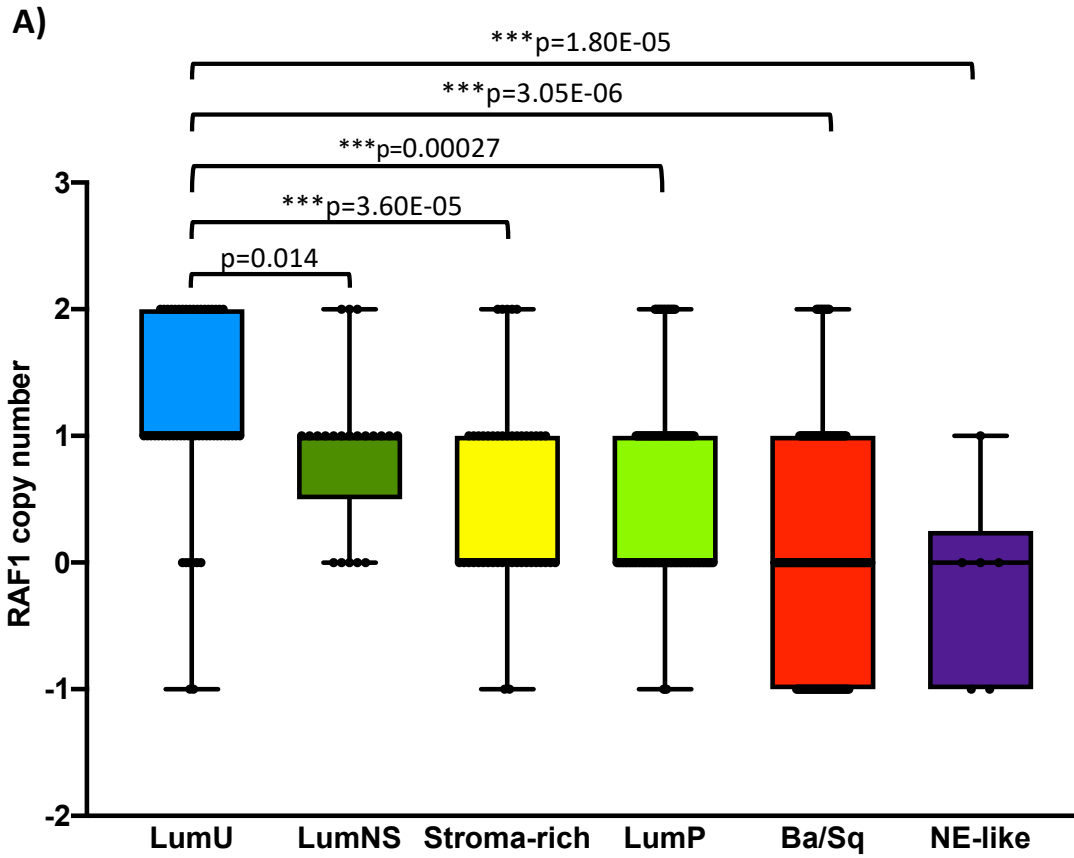
SUPPLEMENTARY INFORMATION

Supplementary Tables 1-7

(see separate accompanying spreadsheet files)

Supplementary Figures 1-19

Supplementary Figure 1

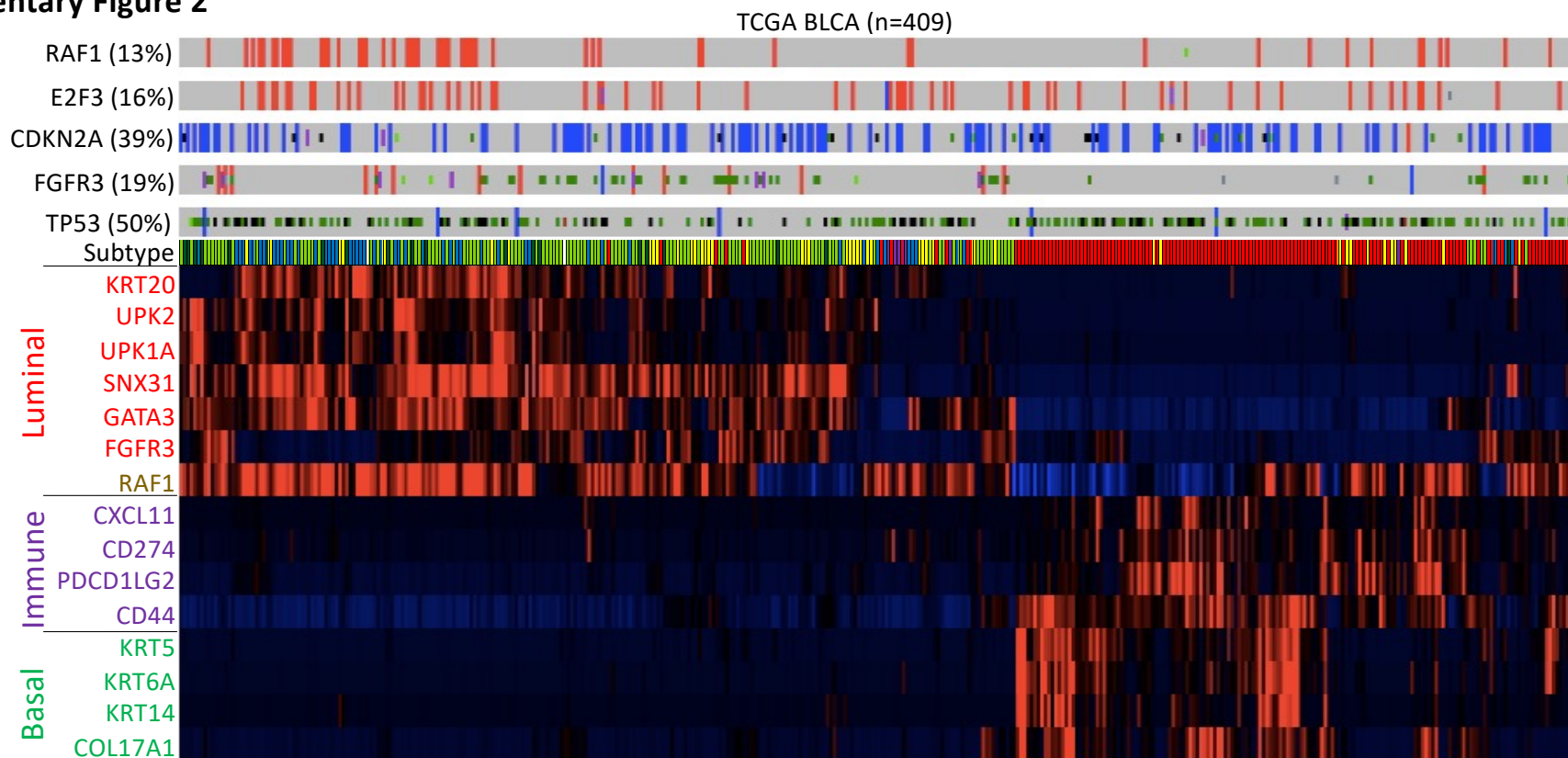


B) Comparison of RAF1 copy-numbers across subtypes

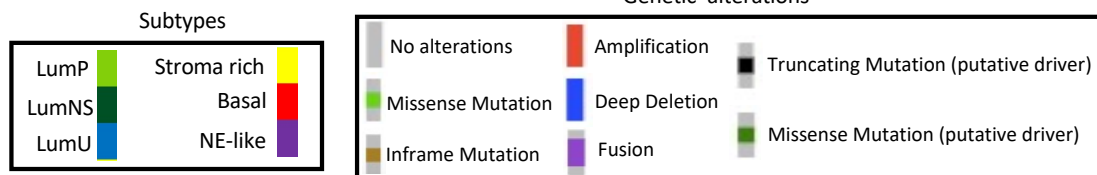
	Ba/Sq	LumNS	LumP	LumU	NE-like	Stroma-rich
Ba/Sq	1					
LumNS	0.024	1				
LumP	0.032	0.34	1			
LumU	3.05E-06	0.014	0.00027	1		
NE-like	0.2	0.0083	0.023	1.80E-05	1	
Stroma-rich	0.29	0.11	0.29	3.60E-05	0.069	1

Supplementary Figure 1: Comparison of *RAF1* copy number across bladder tumor consensus transcriptional subtypes. (A) *RAF1* copy number values for all TCGA bladder tumors that were assigned a consensus subtype (n=406). Values of -1, 0, 1, and 2 correspond to shallow deletion, neutral, gain, and amplification, respectively. (B) Bonferroni-corrected p-values for pair-wise comparisons of *RAF1* copy-number values across bladder cancer subtypes with $p \leq 0.0017$ ($0.05/30$) considered to be statistically significant (highlighted in orange). The luminal unstable (LumU) subtype has significantly more *RAF1* amplified tumors than all other subtypes except for luminal non-specified (LumNS) subtype. LumP, luminal papillary; Ba/Sq, basal-squamous; NE, neuroendocrine.

Supplementary Figure 2

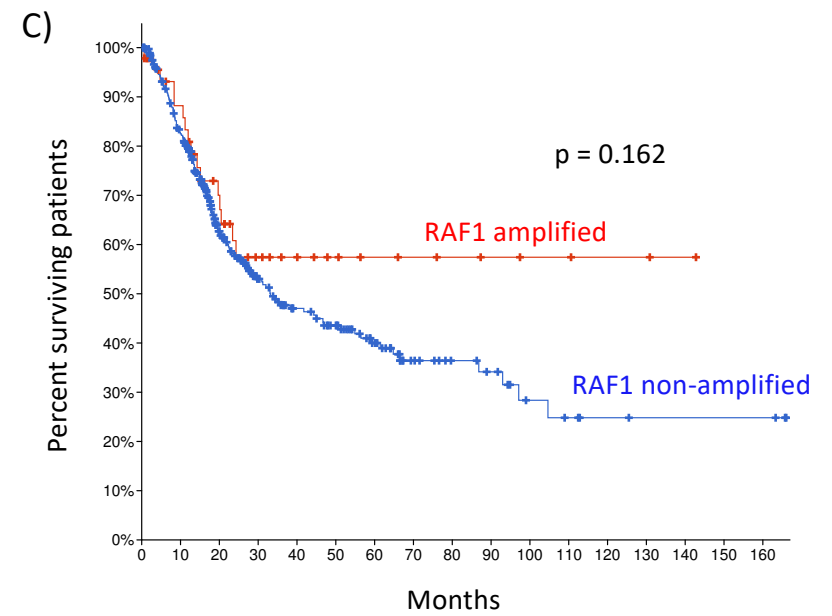
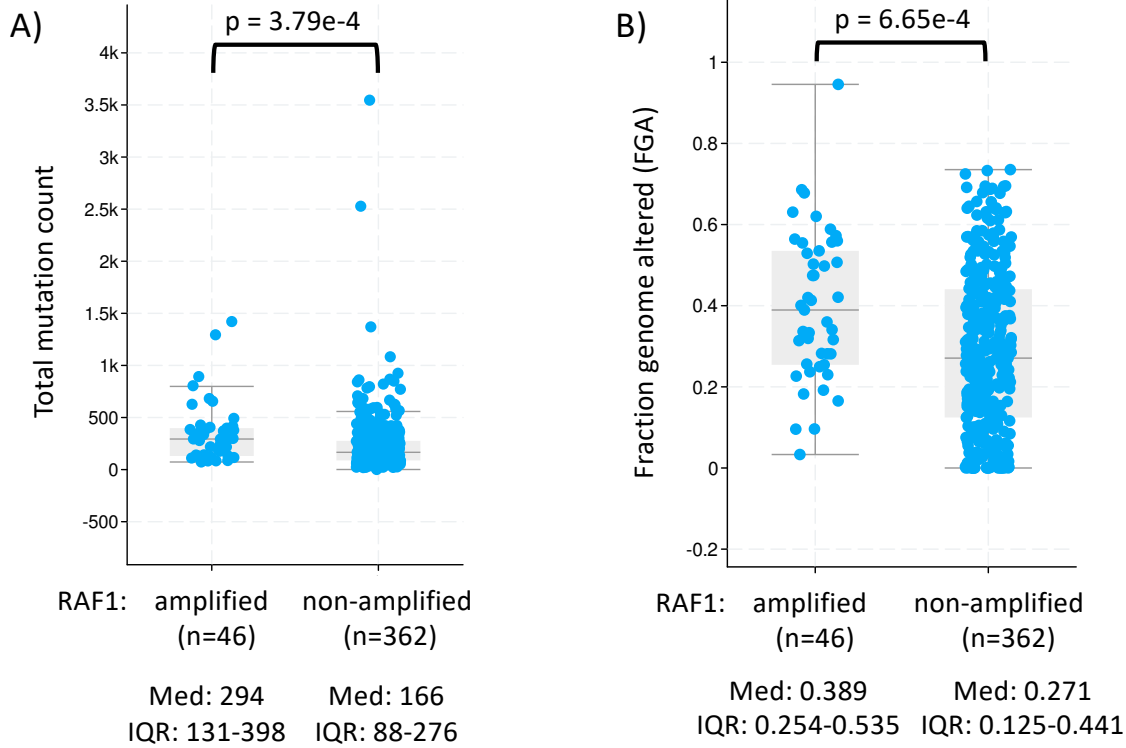


mRNA expression -3 3



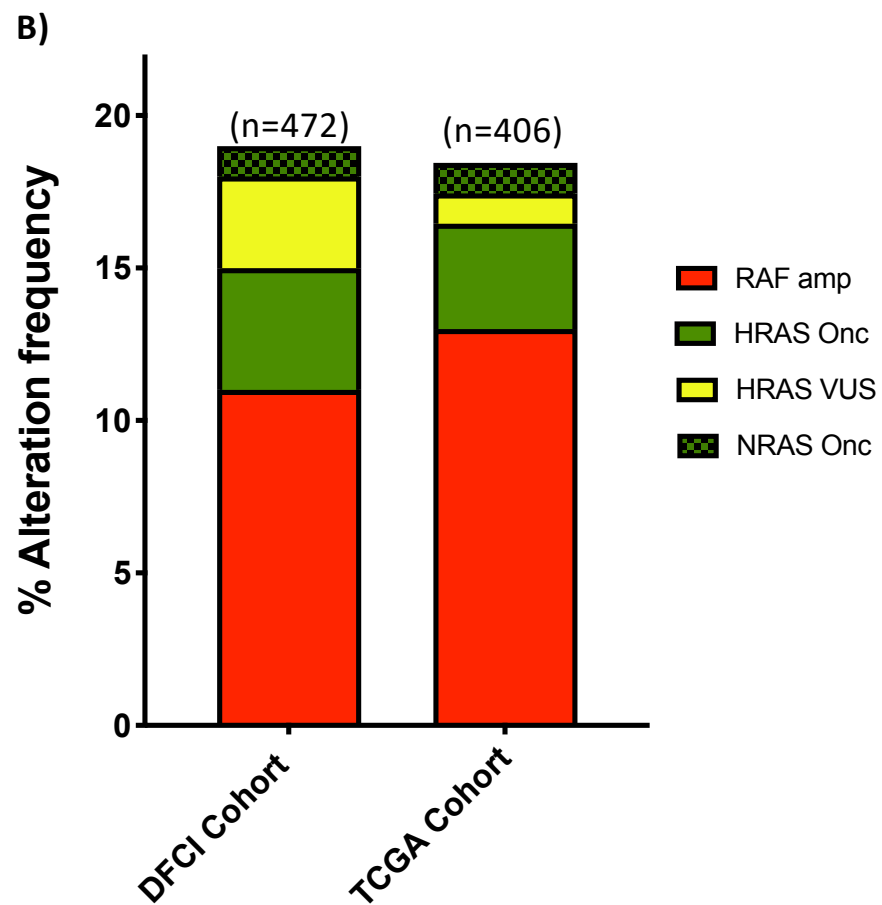
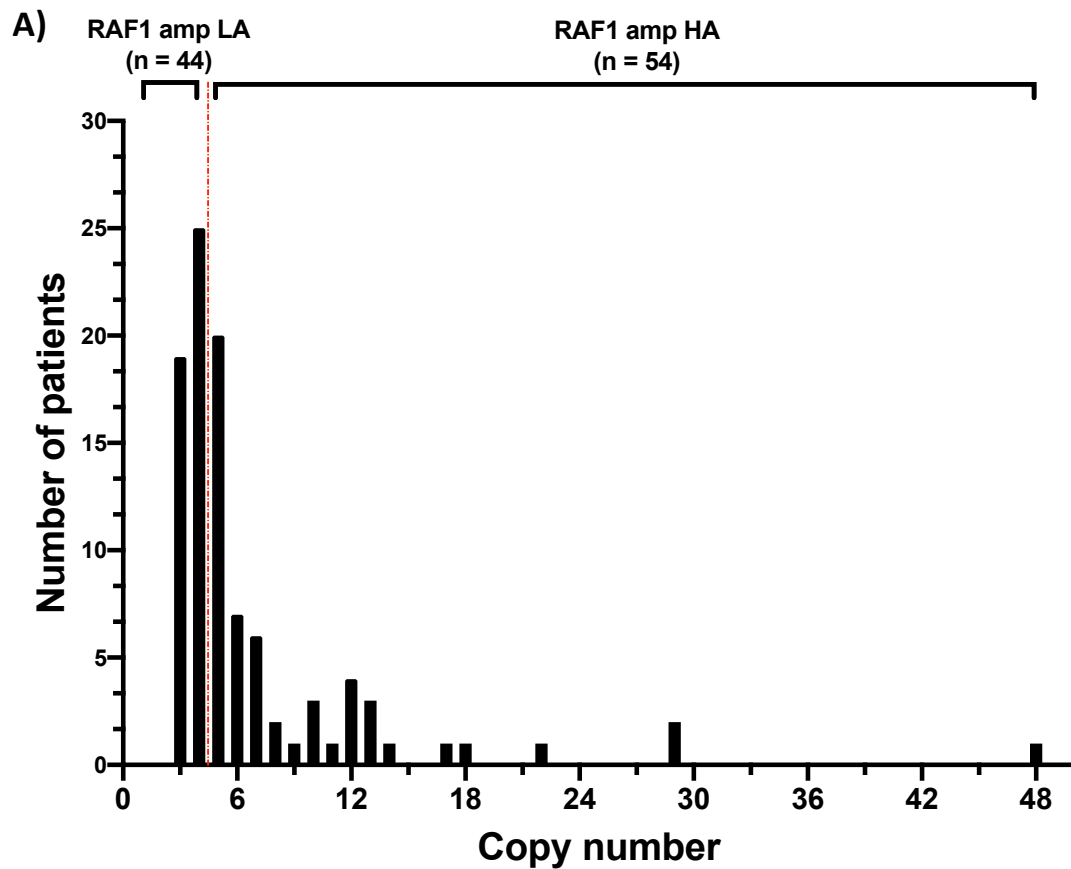
Supplementary Figure 2: Gene alterations, gene expression, and consensus subtype assignments for TCGA bladder cancer cohort (n=409). Alterations in *RAF1* and other gene of interest (*E2F3*, *CDKN2A*, *FGFR3*, and *TP53*) as well as consensus molecular subtype assignments are shown across the top. Expression levels of select luminal, immune, and basal genes are shown in the heatmap. LumU, luminal unstable; LumNS, luminal non-specified; LumP, luminal papillary; Ba/Sq, basal-squamous; NE, neuroendocrine.

Supplementary Figure 3



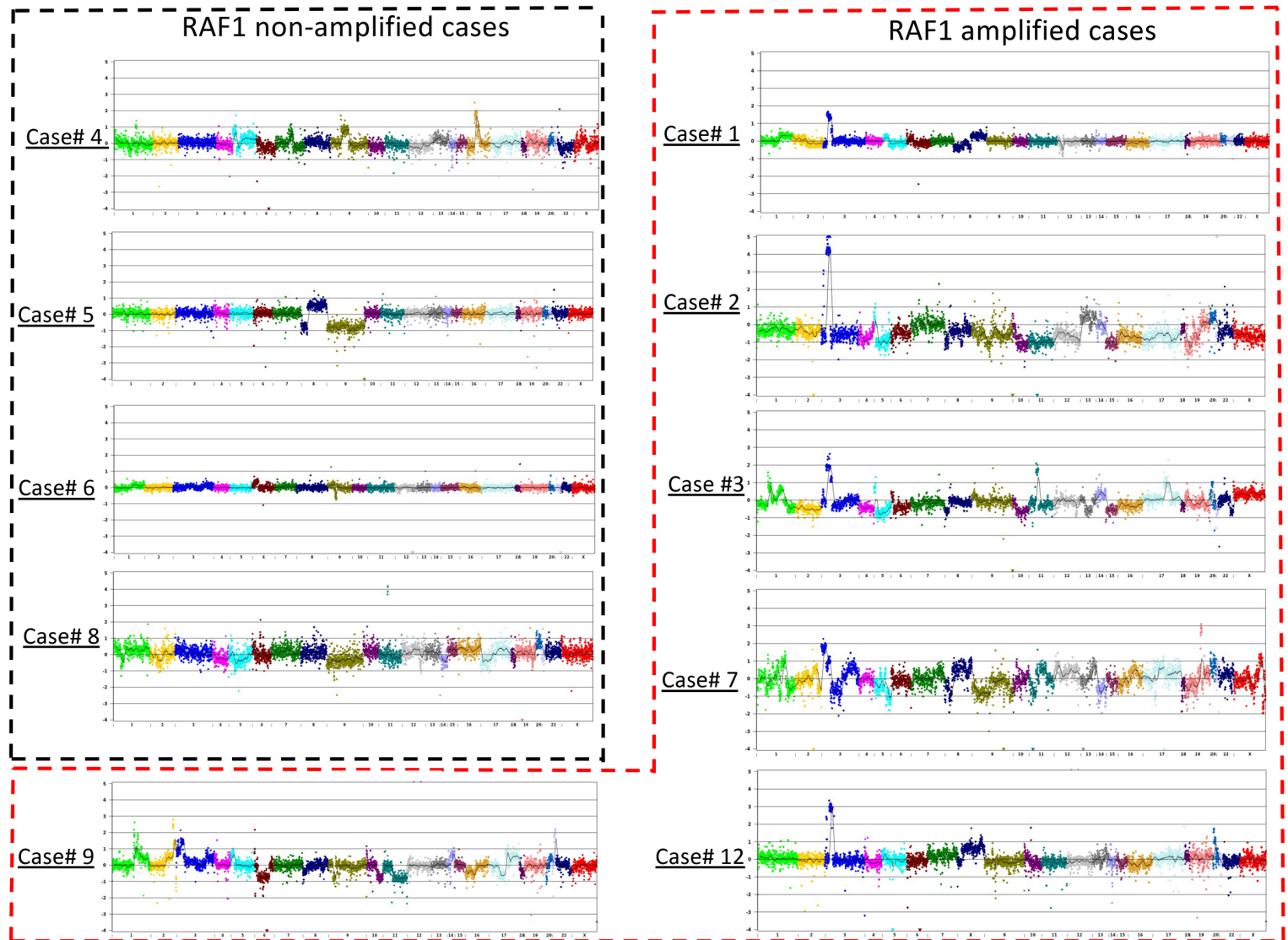
Supplementary Figure 3: Correlation of *RAF1* amplification with genomic features and clinical outcomes in TCGA bladder cancer cohort (n=408). (A) Total mutation count in *RAF1*-amplified tumors is significantly higher than in *RAF1* non-amplified tumors. (B) The fraction genome altered (FGA) is significantly higher in *RAF1*-amplified tumors than in *RAF1* non-amplified tumors. (C) There is no significant difference in overall survival of patients with *RAF1*-amplified versus *RAF1* non-amplified tumors. Data and portions of the images were downloaded from cbioPortal (www.cbioportal.org). P-values for total mutation count and fraction genome altered were calculated using the Kruskal-Wallis method. Overall survival was calculated using the Kaplan-Meier method. Med, median. IQR, inter-quartile range.

Supplementary Figure 4



Supplementary Figure 4: RAF1 and HRAS alterations in the Dana-Farber/Brigham & Women's Cancer Center cohort. (A) Ninety-eight of the 472 cases were identified as having >2 copies of *RAF1* with the estimated number of copies ranging from 3 to 48. Manual review of copy number data was performed and cases were separated into low amplification (LA, 3-4 copies; n=44) or high amplification (HA, ≥ 5 copies; n=54) groups. (B) Bladder tumors from our institutional cohort (n=472) and TCGA (n=406) with *RAF1* amplification (RAF amp), oncogenic HRAS mutation (HRAS Onc), HRAS variant of unknown significance (HRAS VUS), or oncogenic NRAS mutation (NRAS Onc). For the institutional cohort, the RAF1 amp group includes tumors with ≥ 5 copies of RAF1.

Supplementary Figure 5

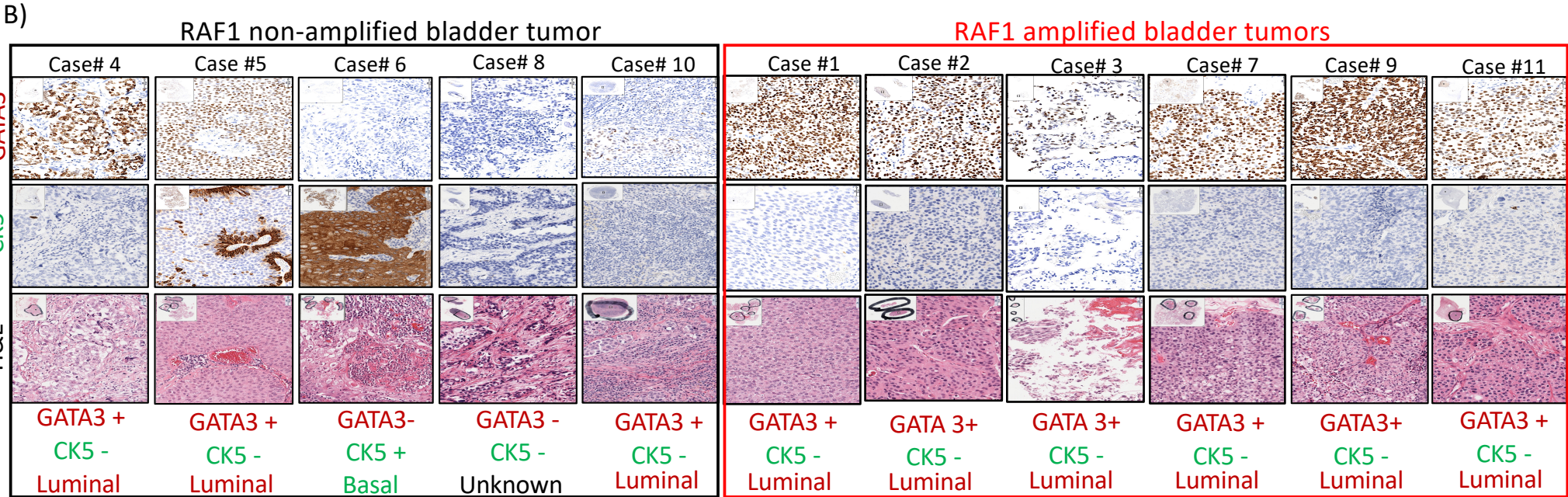


Supplementary Figure 5: Copy-number plots for select *RAF1*-amplified and *RAF1* non-amplified bladder tumors from the Brigham & Women's/Dana-Farber Cancer Center. *RAF1* status was identified from available targeted next-generation sequencing data.²⁹ Select cases with *RAF1* amplifications (within red hatched box) as well as clinically matched cases without *RAF1* amplification (within black hatched box) were identified by manual review of copy-number data. The *RAF1* gene is located on chromosome 3 (dark blue), and amplification of the portion of chromosome 3p harboring the *RAF1* locus is evident in *RAF1*-amplified cases (cases 1, 2, 3, 7, 9, and 12). Plots for cases 1-4 were also shown in figure 2A.

Supplementary Figure 6

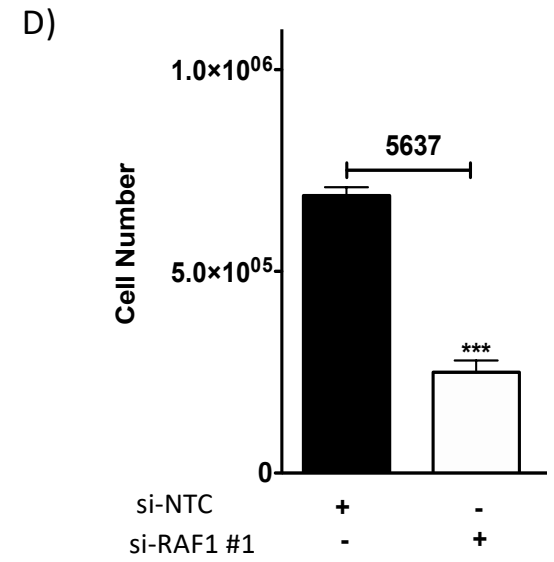
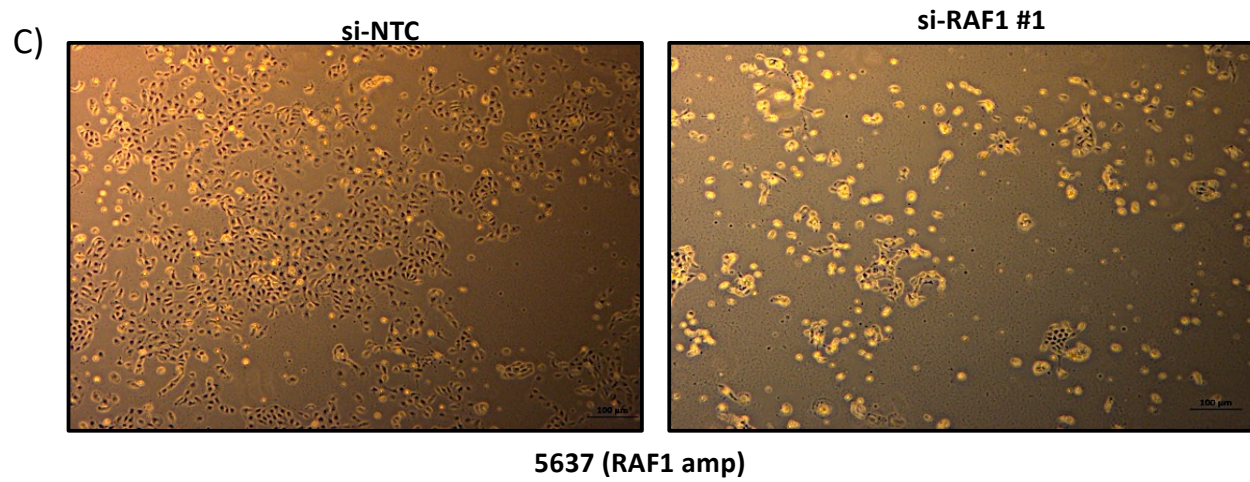
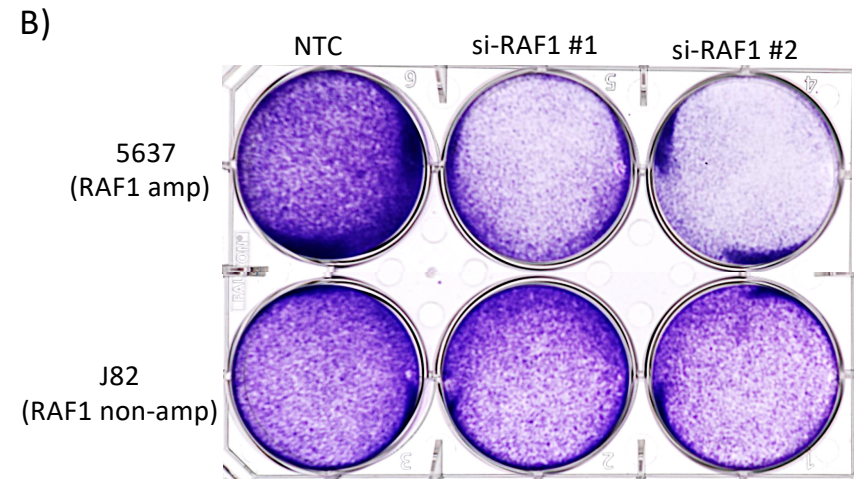
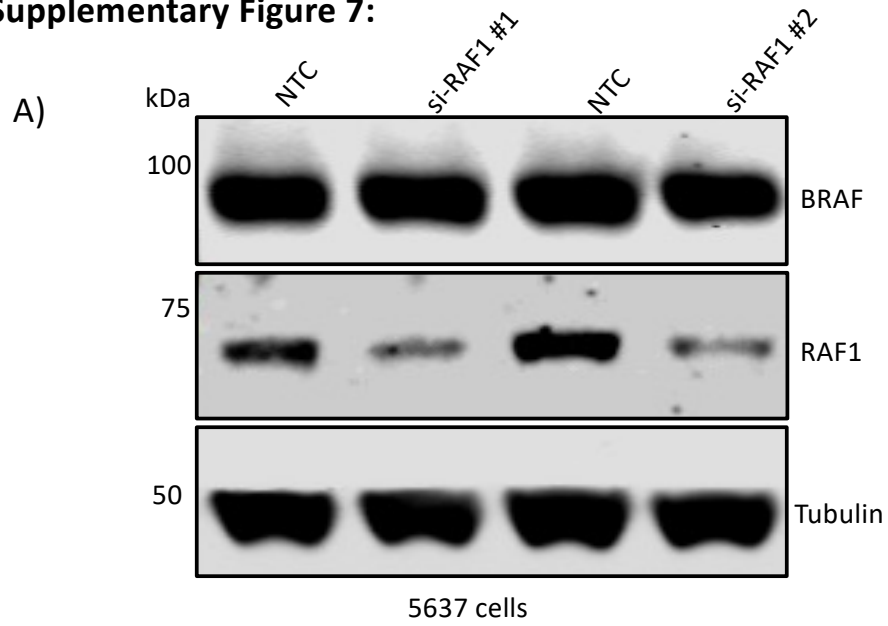
A)

	RAF1 amplified patients		
Per 100 nuclei analyzed	Case 1	Case 2	Case 3
RAF1=CEP3	1	0	10
RAF1<CEP3	0	0	0
RAF1>CEP3	99	100	90



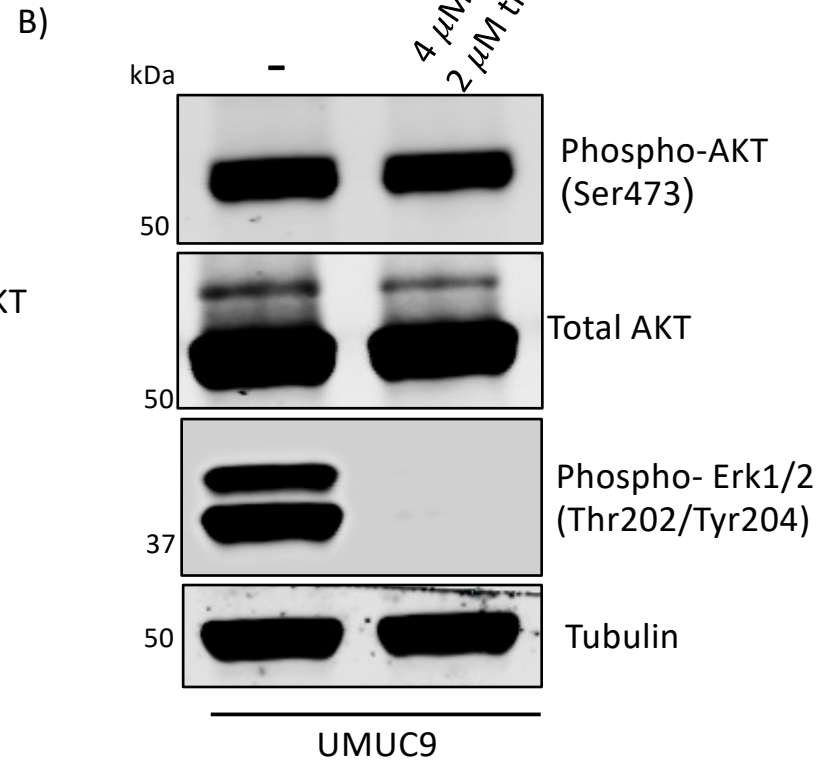
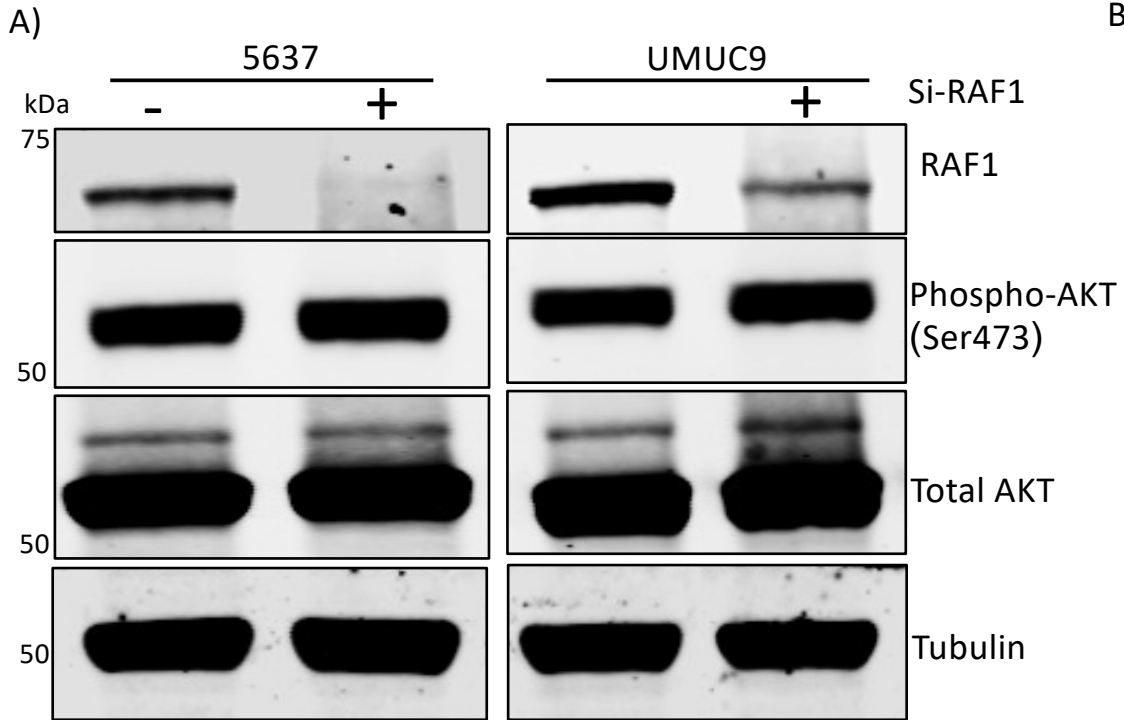
Supplementary Figure 6: FISH and IHC analysis of *RAF1*-amplified and *RAF1* non-amplified cases from the Brigham & Women's/Dana-Farber Cancer Center. (A) Quantification of FISH data for *RAF1*-amplified cases 1, 2, and 3. For each case, the number of *RAF1* foci and number of centromere 3 (CEP3) foci were counted in 100 tumor cells. In each case, the majority (90-100 out of 100) of tumor cells had more *RAF1* foci than CEP3 foci, consistent with *RAF1* amplification as a clonal event in these tumors. (B) For each *RAF1*-amplified and non-amplified case, H&E-stained slides from the tumor specimen were reviewed by a pathologist to identify areas of highest tumor density. Slides from this region were stained for the luminal marker GATA3 and the basal marker CK5 and images acquired at 20X magnification. All *RAF1*-amplified tumors and nearly all of the clinically matched *RAF1* non-amplified tumors were positive for GATA3 and negative for CK5, consistent with a luminal phenotype. H&E, GATA3, and CK5 images for cases 1-4 were also shown in figure 2B.

Supplementary Figure 7:



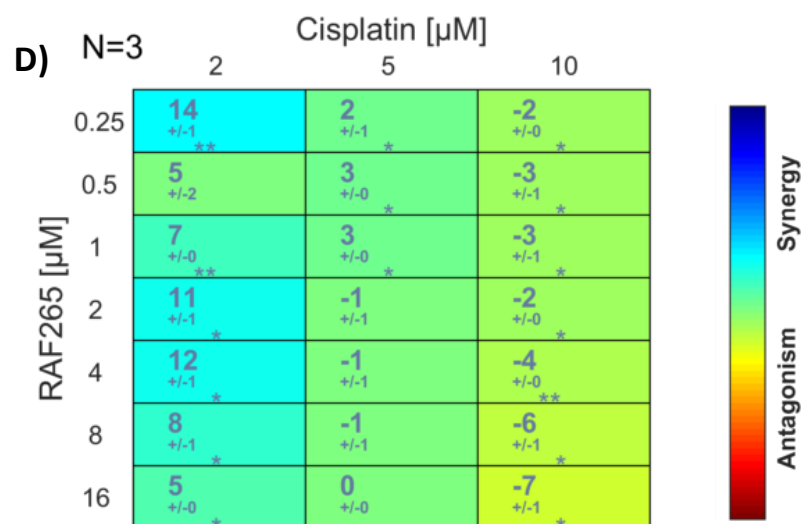
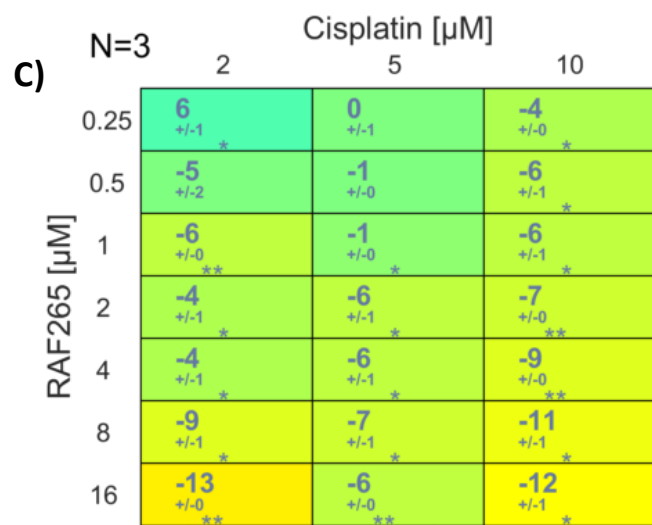
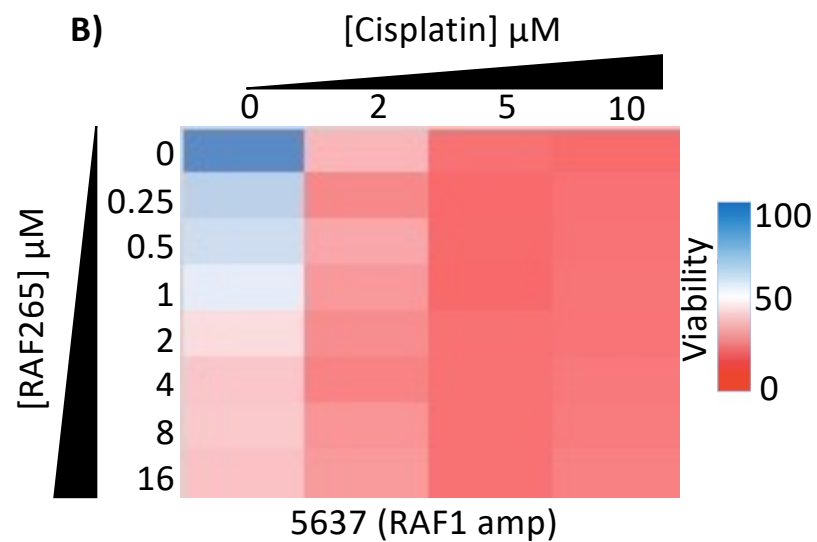
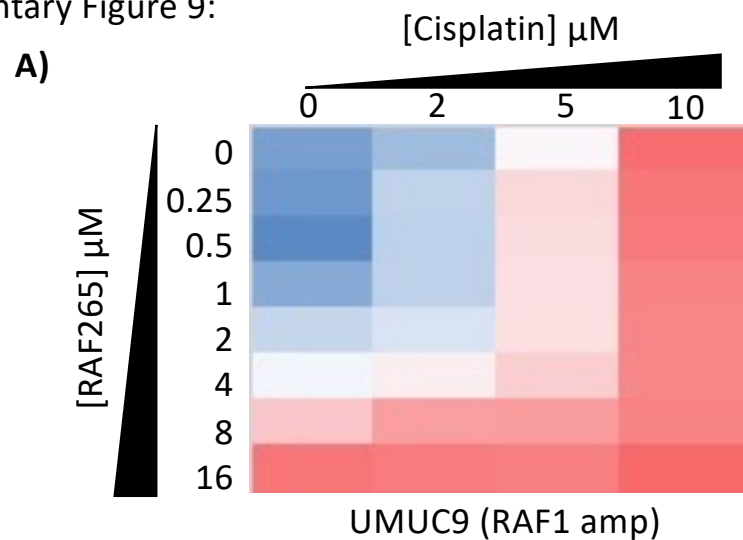
Supplementary Figure 7: *RAF1* depletion has a greater impact on cell growth and viability of *RAF1*-amplified than *RAF1* non-amplified bladder cancer cells. (A) Immunoblot showing two different siRNAs (si*RAF1* #1 and si*RAF1* #2) used to deplete *RAF1* in the *RAF1*-amplified 5637 cell line. BRAF levels were not impacted by siRNA-mediated depletion of *RAF1*(blots were run in parallel from the same sample). (B) 5637 cells were significantly more sensitive to *RAF1* depletion than the *RAF1* non-amplified J82 cell line. Viability was measured by crystal violet staining of cells 72 hours following *RAF1* depletion. (C) Phase-contrast microscopy images obtained after *RAF1* depletion shows morphological features of cell death in the *RAF1*-amplified 5637 cell line. (D) *RAF1* depletion results in significant growth delay in *RAF1*-amplified 5637 cells as measured by cell number count. Significant differences were calculated by unpaired two-tailed Student's t test and denoted by asterisks.

Supplementary Figure 8:



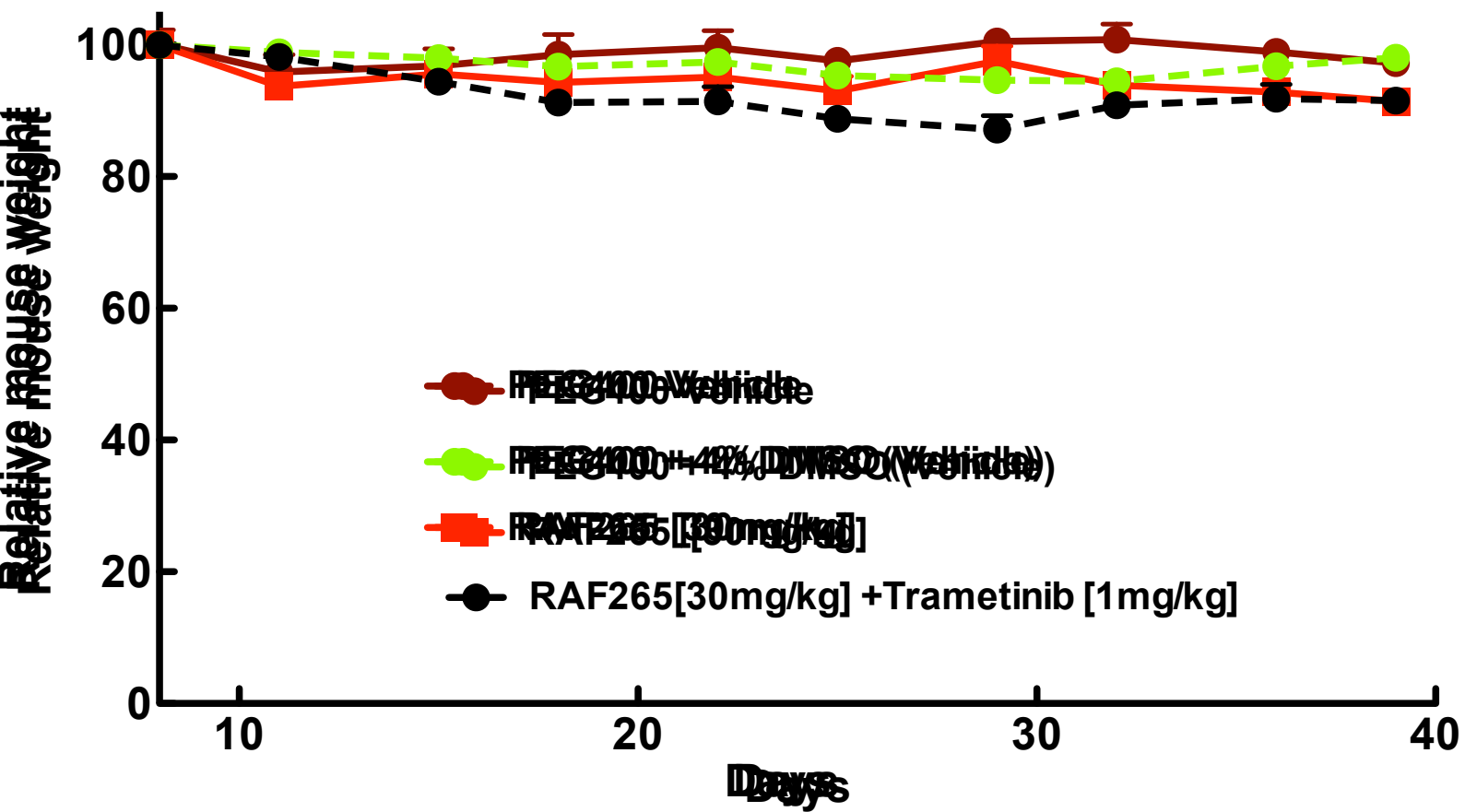
Supplementary Figure 8: RAF1 depletion or inhibition inhibits ERK phosphorylation but does not impact AKT phosphorylation. (A) *RAF1* depletion by siRNA does not affect the levels of phosphorylated AKT in *RAF1* amplified bladder cancer cell lines 5637 and UMUC9. (B) Treatment with the combination of RAF265 and trametinib in UMUC9 cells completely abrogates phosphorylated ERK but does not impact the levels of phosphorylated AKT. Immunoblots were run in parallel from the same sample.

Supplementary Figure 9:



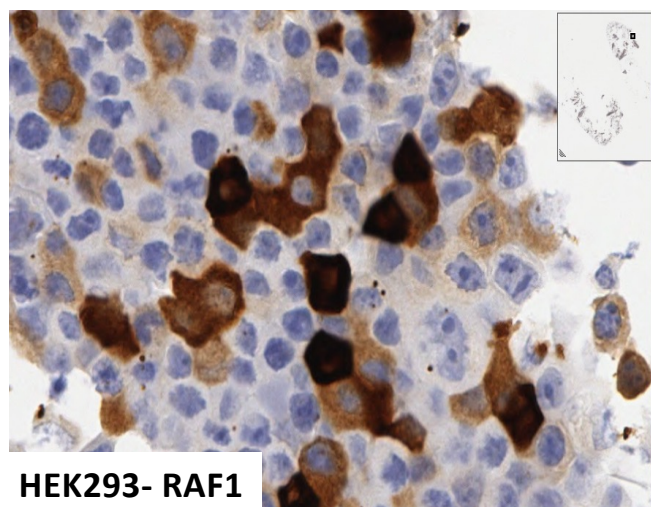
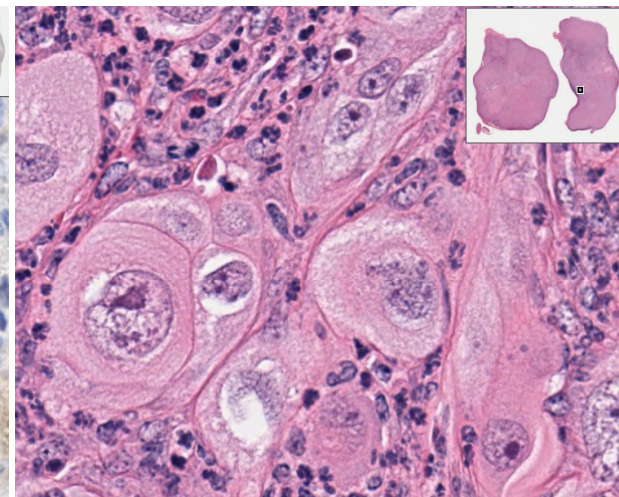
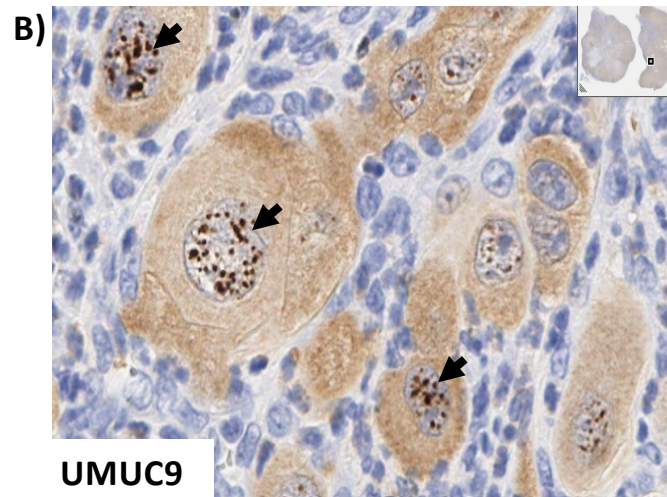
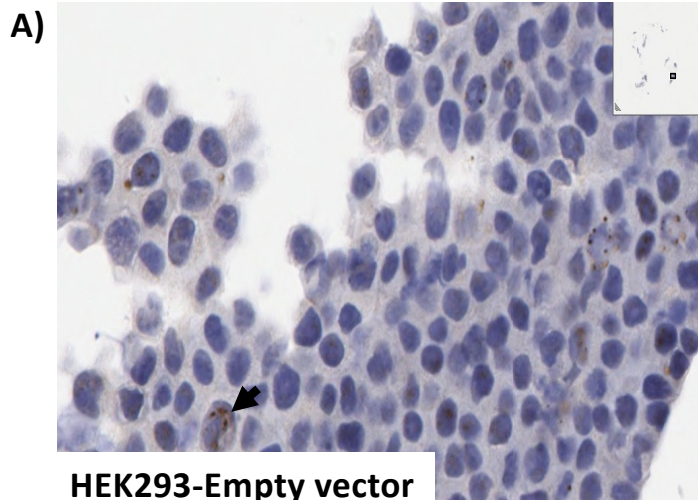
Supplementary Figure 9: Effect of cisplatin and RAF265 combination treatment on survival of RAF1-amplified bladder cancer cell lines. (A) Heat map showing the viability of the *RAF1*-amplified bladder cancer cell lines UMUC9 (left) and 5637 (right) following 3-day treatment with combinations of cisplatin (0-10 μ M) and the RAF inhibitor RAF265 (0-16 μ M). (B) The Combenefit software package was used to calculate the level of synergy/antagonism across the drug dose ranges for both UMUC9 (left) and 5637 (right). Additive toxicity was observed across most drug concentrations although mild synergy was observed at low cisplatin concentrations in the 5637 cell line.

Supplementary Figure 10

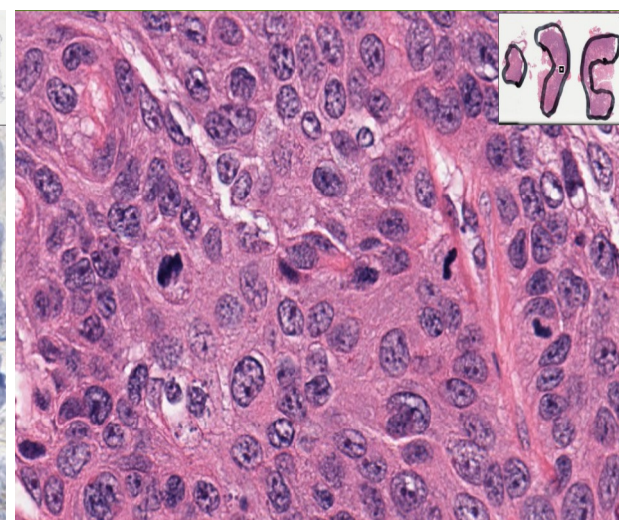
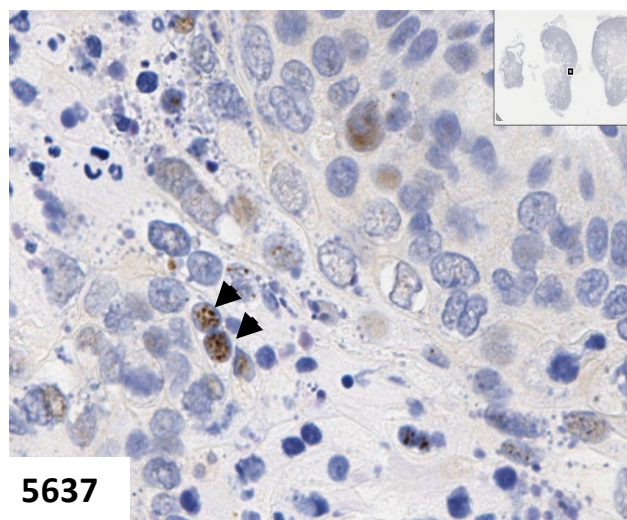


Supplementary Figure 10: RAF265 and RAF265 plus trametinib are well-tolerated in RAF1-amplified tumor-bearing mice. Mice bearing UMUC9 xenografts were treated twice weekly for a maximum of nine intraperitoneal injections with the RAF inhibitor RAF265 (30 mg/kg) alone or in combination with the MEK inhibitor trametinib (1 mg/kg). Mouse body weight was recorded prior to each drug treatment ($n \geq 8$ mice per group).

Supplementary Figure 11

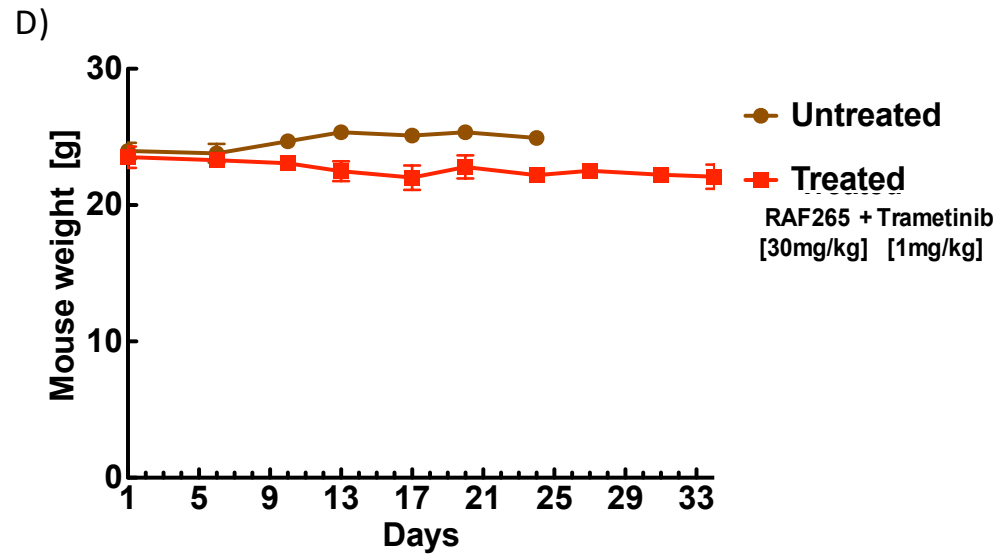
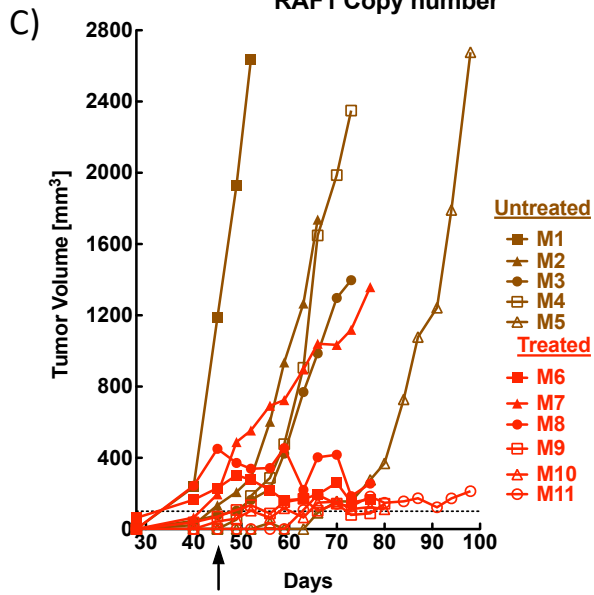
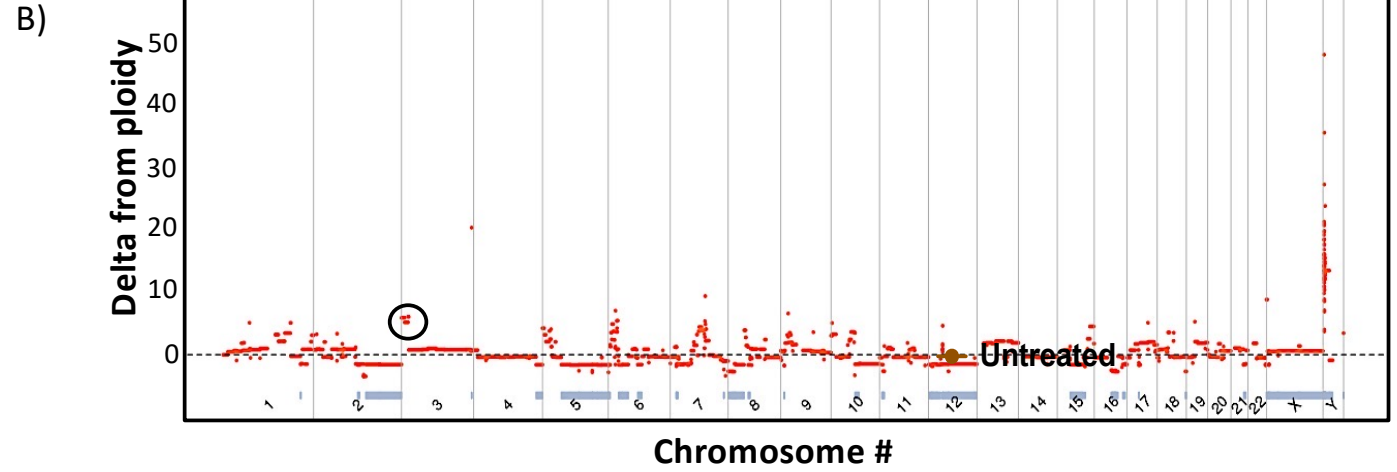
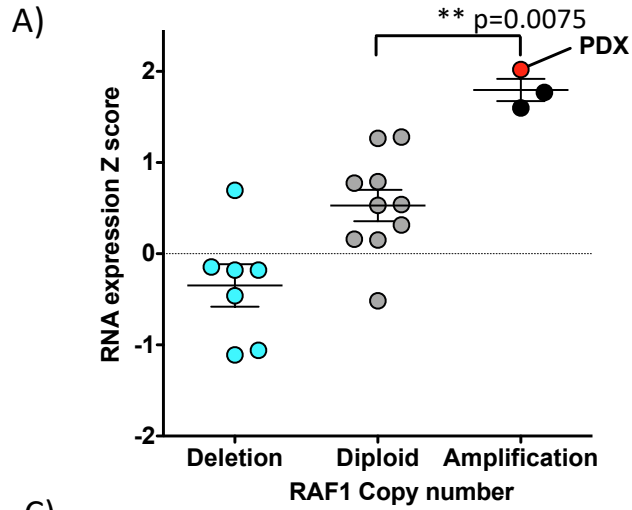


RAF1 ab (Sigma HPA002640, 1:50)



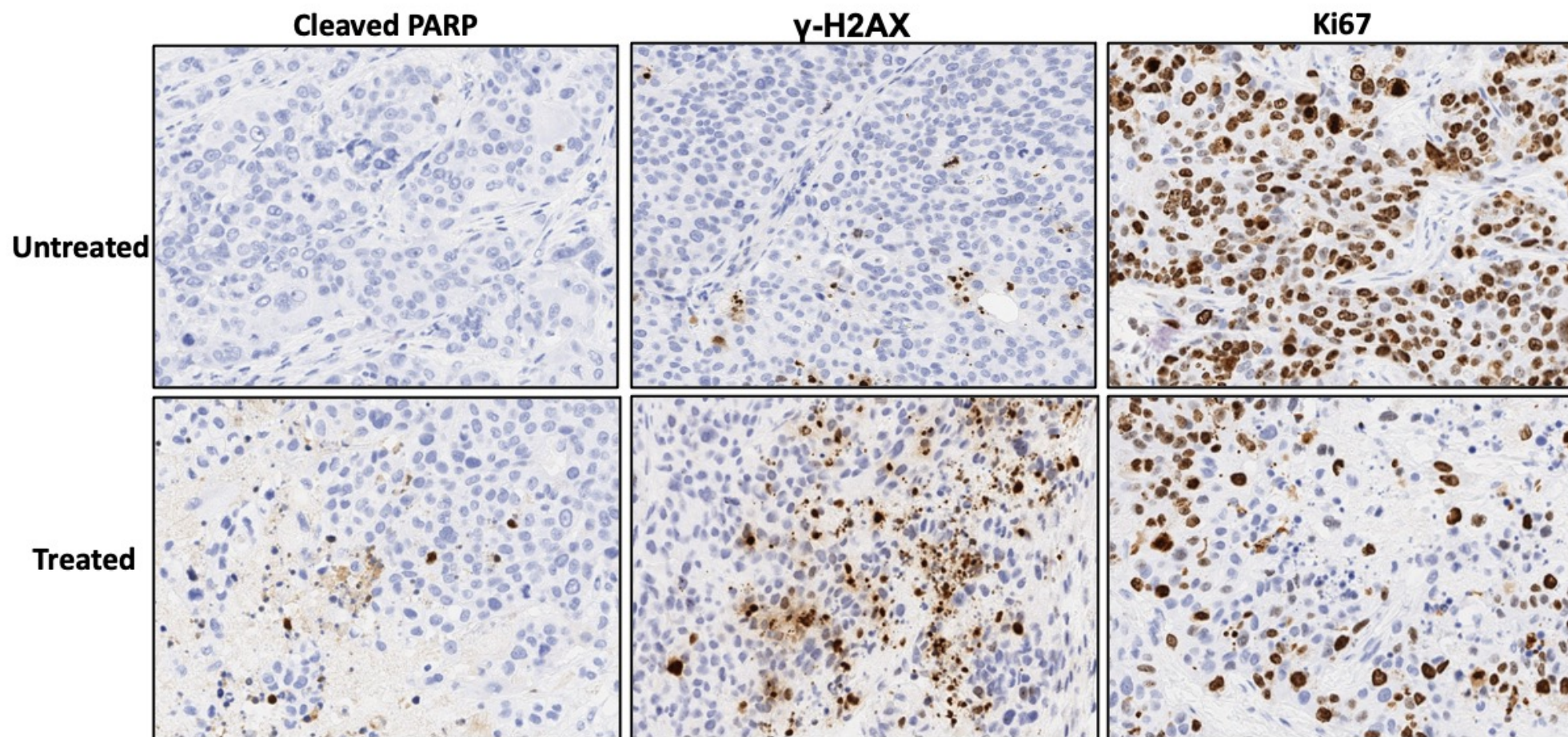
Supplementary Figure 11: Immunohistochemical (IHC) detection of RAF1 in *RAF1*-amplified tumor xenografts. (A) HEK293T cells transfected with empty vector (top) or wild-type *RAF1* (bottom) were used to validate RAF1 staining by IHC. (B) *RAF1*-amplified cell line xenografts (5637 and UMUC9) were resected, fixed, and stained for *RAF1*. Images were acquired at 20-40X magnification.

Supplementary Figure 12:



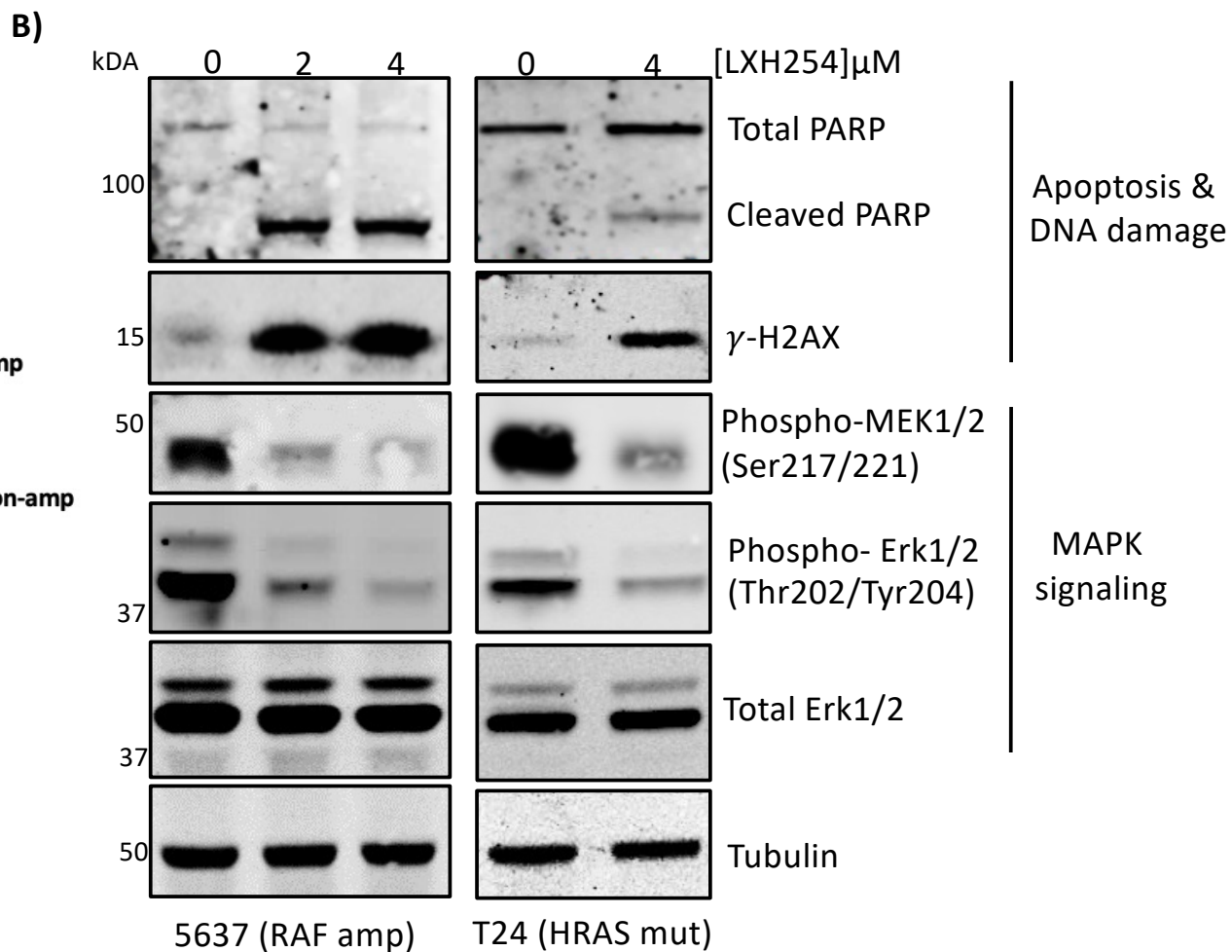
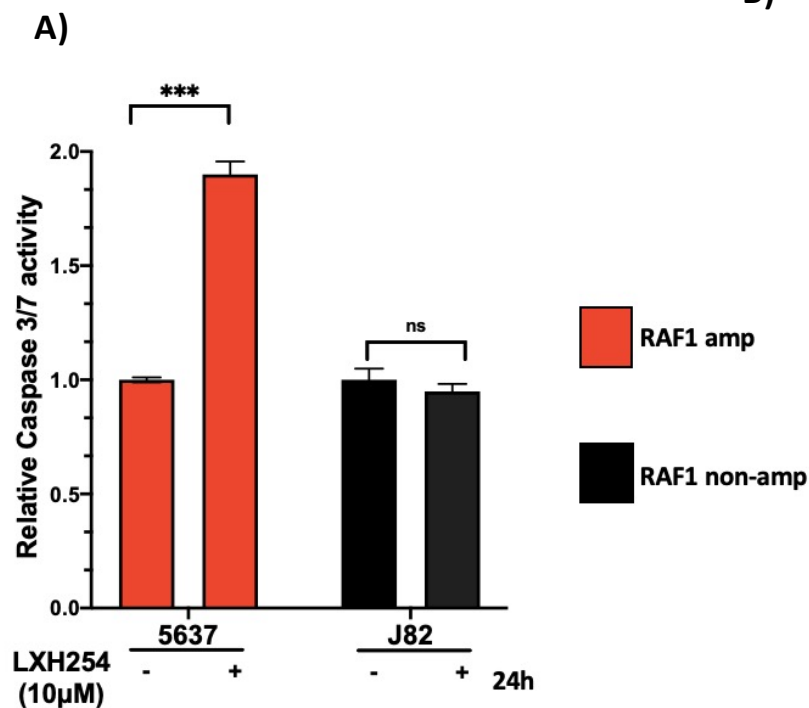
Supplementary Figure 12: A *RAF1*-amplified patient-derived bladder tumor xenograft (PDX) model is sensitive to combined RAF plus MEK inhibition. (A) *RAF1* gene expression Z-score (y-axis) versus DNA copy number (x-axis) for commercially available PDX bladder tumor models. The PDX model with the highest *RAF1* gene expression Z-score (TM00024/BL0440F; highlighted in red) was selected for this project. **p=0.0075, by ANOVA with Bonferroni's post hoc test. (B) Copy-number data for the selected *RAF1*-amplified bladder tumor PDX model. The amplified region of chromosome 3 containing the *RAF1* gene is circled. Data used to create graphs in panels A and B were retrieved from the Mouse Models of Human Cancer Database (MMHCdb), Mouse Genome Informatics, The Jackson Laboratory, Bar Harbor, Maine. (<http://tumor.informatics.jax.org>, 2020). (C) Tumor volume measurements for each PDX-implanted mouse beginning 30 days post-implantation. Treatment was started at day 45 (denoted by black arrow) or as soon thereafter as tumors reached 100 mm³ in size (indicated by the horizontal black dashed line). (D) Body weight measurements for mice in the treated and untreated groups.

Supplementary Figure 13:



Supplementary Figure 13: *RAF1*-amplified patient-derived bladder tumor xenograft (PDX) model shows evidence of apoptosis and decreased proliferation after RAF plus MEK inhibition. Immunohistochemical staining of cleaved PARP (apoptosis marker) and γ H2AX (DNA damage marker) are increased and staining of Ki-67 (proliferation marker) is decreased following RAF plus MEK inhibitor treatment compared to untreated tumors. Images were acquired at 20X magnification.

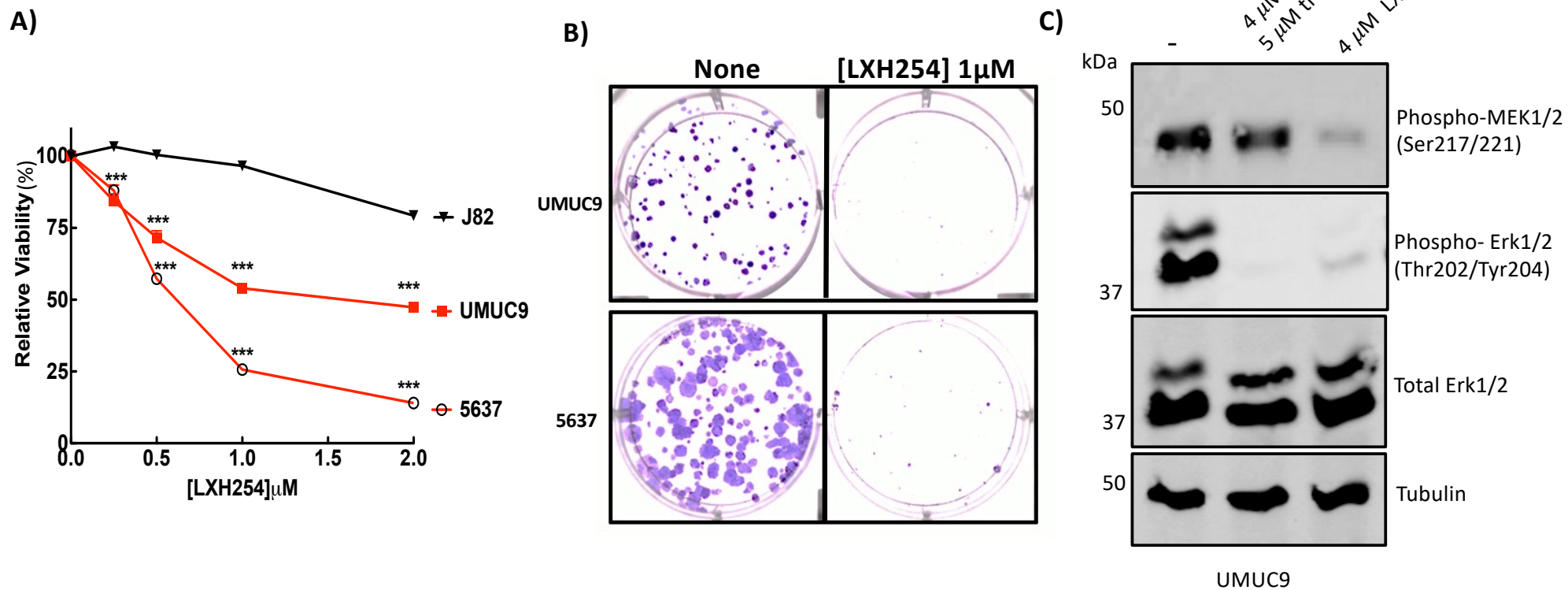
Supplementary Figure 14



Supplementary Figure 14: RAF inhibition induces apoptosis in *RAF1*-amplified and *HRAS*-mutant bladder cancer cells. (A) The *RAF1*-amplified bladder cancer cell line 5637 and the *RAF1* non-amplified bladder cancer cell line J82 were treated with 10 μ M of *RAF1* inhibitor LXH254 for 24 hours followed by measurement of caspase 3/7 activity. LXH254 treatment induced a significant increase in caspase 3/7 activity in 5637 cells, indicative of apoptosis, while having no impact on J82 cells. Significant differences were calculated by unpaired two-tailed Student's t test and denoted by asterisks. (B) The *RAF1*-amplified 5637 and the *HRAS*-mutant T24 bladder cancer cell lines were treated with LXH254 (0-4 μ M) for 24 hours and cell lysates were harvested for immunoblotting. LXH254 treatment inhibited MAPK signaling as measured by decreased levels of phosphorylated MEK and ERK. In addition, LXH254 treatment led to increased levels of the DNA damage marker γ -H2AX and the apoptosis marker cleaved PARP, consistent with LXH254-induced apoptotic cell death. Immunoblots were run in parallel from the same sample.

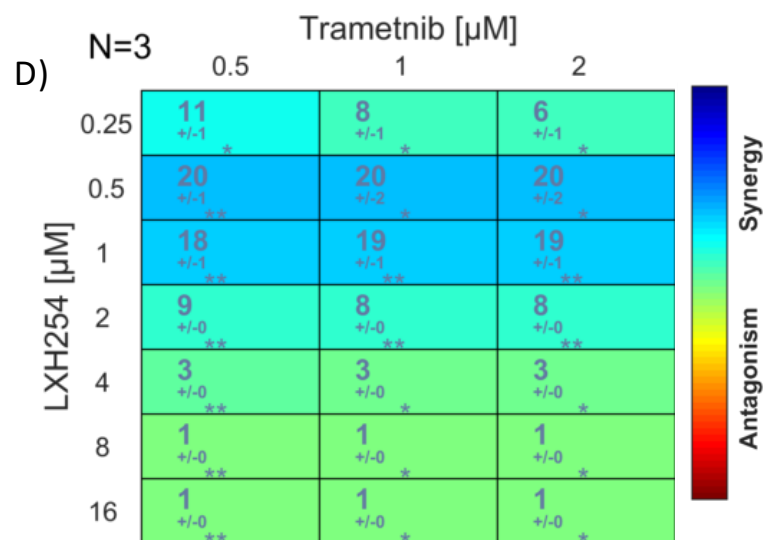
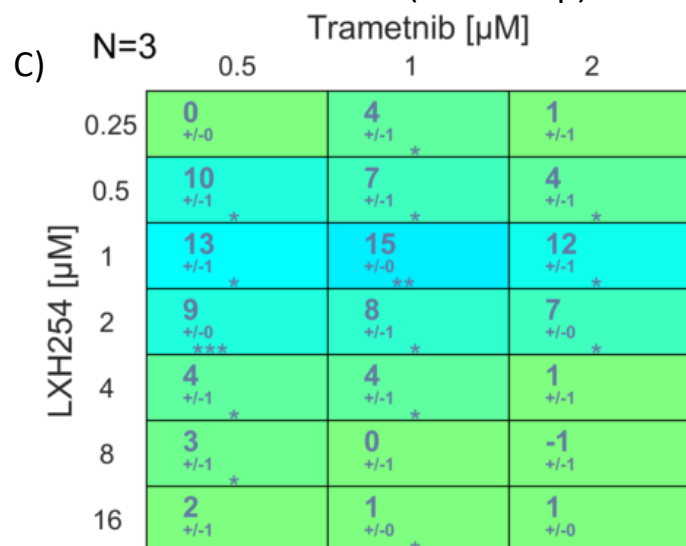
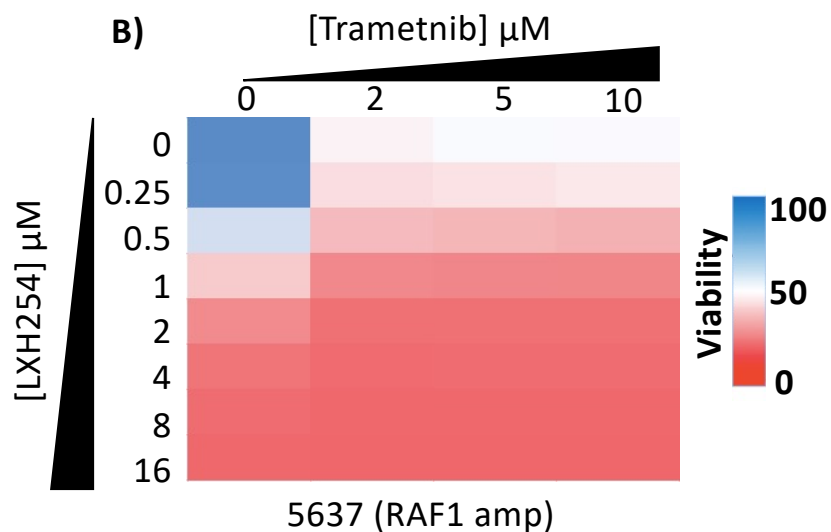
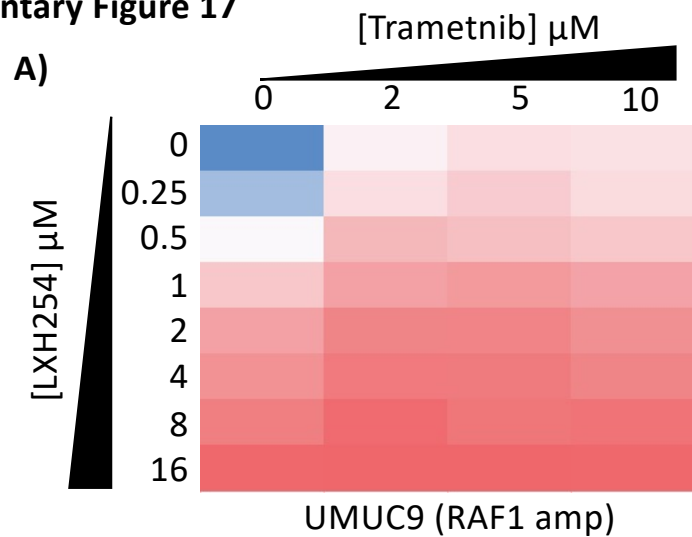
Supplementary Figure 15: *HRAS* and *NRAS* mutant bladder cancer cell lines are sensitive to RAF1-targeting agents. Viability of T24 (*HRAS* G12V) and Ku-19-19 (*NRAS* Q61R) cells 3 days after treatment with increasing concentrations of (A) RAF265 or (B) LXH254. Significant differences were calculated by ANOVA with Bonferroni's post hoc test and denoted by asterisks, *** $p < 0.0001$. (C) Crystal violet staining 3 days after treatment of T24 cells with LXH254. (D) Colony formation assays in *HRAS*-mutant T24 cells treated with LXH254 and trametinib alone or in combination demonstrates increased sensitivity to the combination. (E) Immunoblot showing inhibition of RAS/RAF/MEK signaling in Ku-19-19 and J82 cells following 24-hour treatment with RAF265 alone or in combination with trametinib.

Supplementary Figure 16



Supplementary Figure 16: LXH254 potently inhibits the viability and growth of *RAF1*-amplified cell lines and blocks RAF/MEK/ERK signaling. (A) Cell viability measured by luminescence following 3-day treatment with the RAF inhibitor LXH254 shows increased sensitivity of *RAF1*-amplified cell lines 5637 and UMUC9 compared to the *RAF1* non-amplified J82 cell line. Significant differences were calculated by ANOVA with Bonferroni's post hoc test and denoted by asterisks. (B) Two-week colony formation assay for *RAF1*-amplified cell lines UMUC9 and 5637 treated with LXH254. (C) Immunoblot of *RAF1*-amplified UMUC9 cells 24 hours following treatment with LXH254 or RAF265 plus trametinib shows that LXH254 efficiently blocks ERK phosphorylation as a single agent owing to its more potent inhibition of MEK phosphorylation.

Supplementary Figure 17

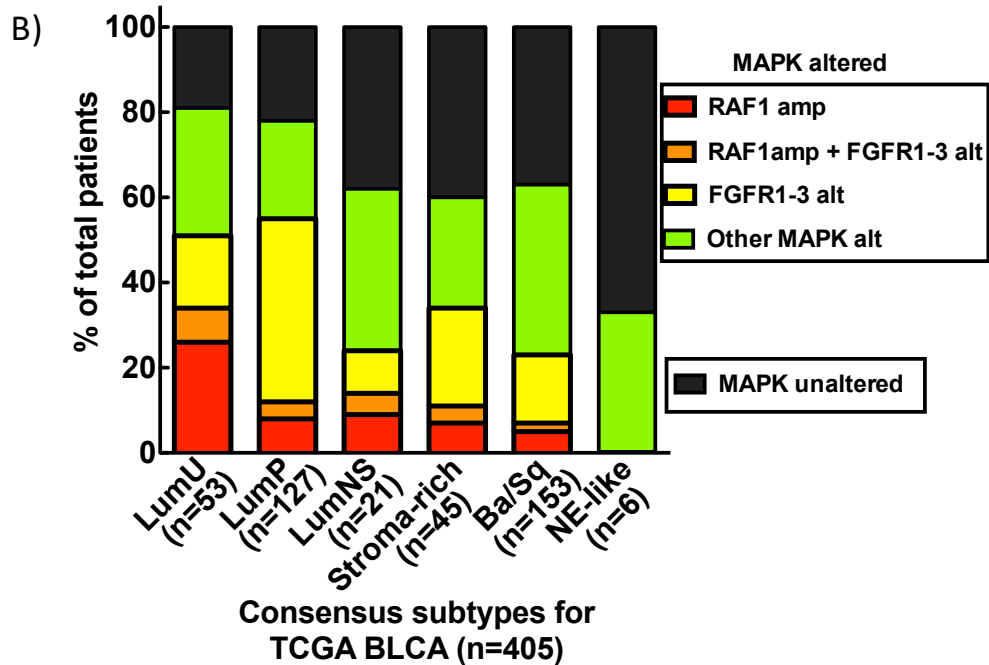
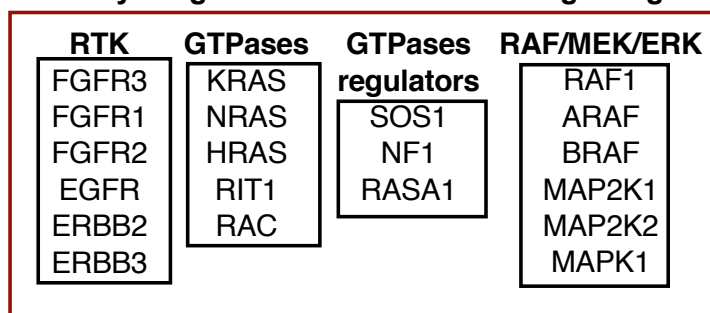


Supplementary Figure 17: Effect of LHX254 and trametinib combination treatment on bladder cancer cell survival. (A) Heat map showing the viability of *RAF1*-amplified bladder cancer cell lines UMUC9 (left) and 5637 (right) following 3-day treatment with combinations of LHX254 (0.25-16 μ M) and trametinib (2-10 μ M). (B) The Combenefit software package was used to calculate the level of synergy/antagonism across the drug dose ranges in UMUC9 (left) and 5637 (right) cell lines. Synergy was observed at low LHX254 concentrations, particularly in the 5637 cell line.

Supplementary Figure 18: *NRAS* mutant Ku-19-19 xenografts are sensitive to RAF1-directed therapy. (A). Mice bearing *NRAS* mutant Ku-19-19 xenografts were treated with the RAF inhibitor LXH254 (15mg/kg or 30mg/kg) or with the combination of RAF265 (30mg/kg) plus trametinib (1mg/kg) beginning 7 days following tumor implantation. The experiment was stopped 14 days after the first treatment because untreated mice had uncontrolled tumor growth (highlighted in hatched boxes) with associated emaciation (arrows). (B) Body weight measurements for treated and untreated mice. (C) Mice bearing *NRAS* mutant Ku-19-19 xenografts treated with trametinib showed a marked decrease in tumor weight, consistent with previous reports in melanoma that *NRAS*-mutant tumors respond to MEK inhibition.

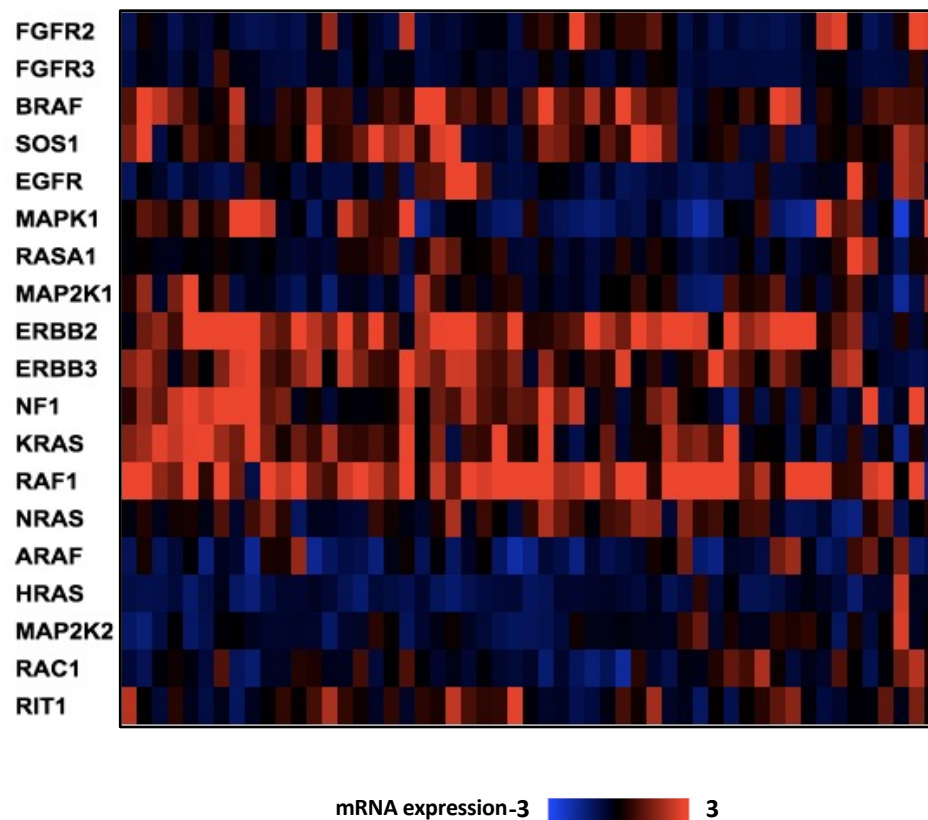
Supplementary Figure 19

A) Analyzed genes involved in MAPK signaling

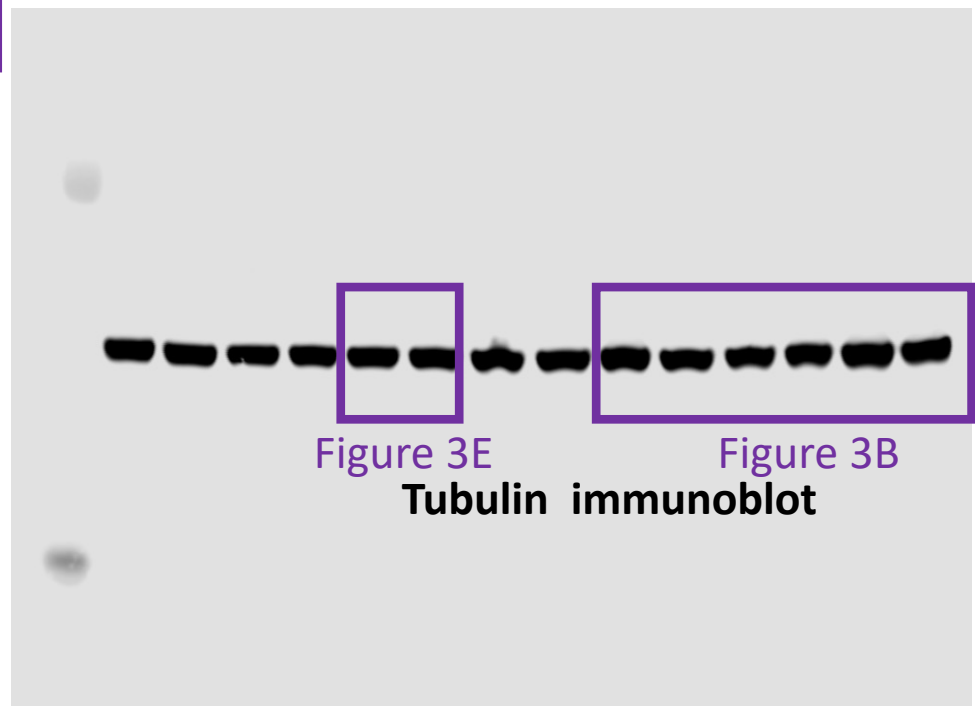
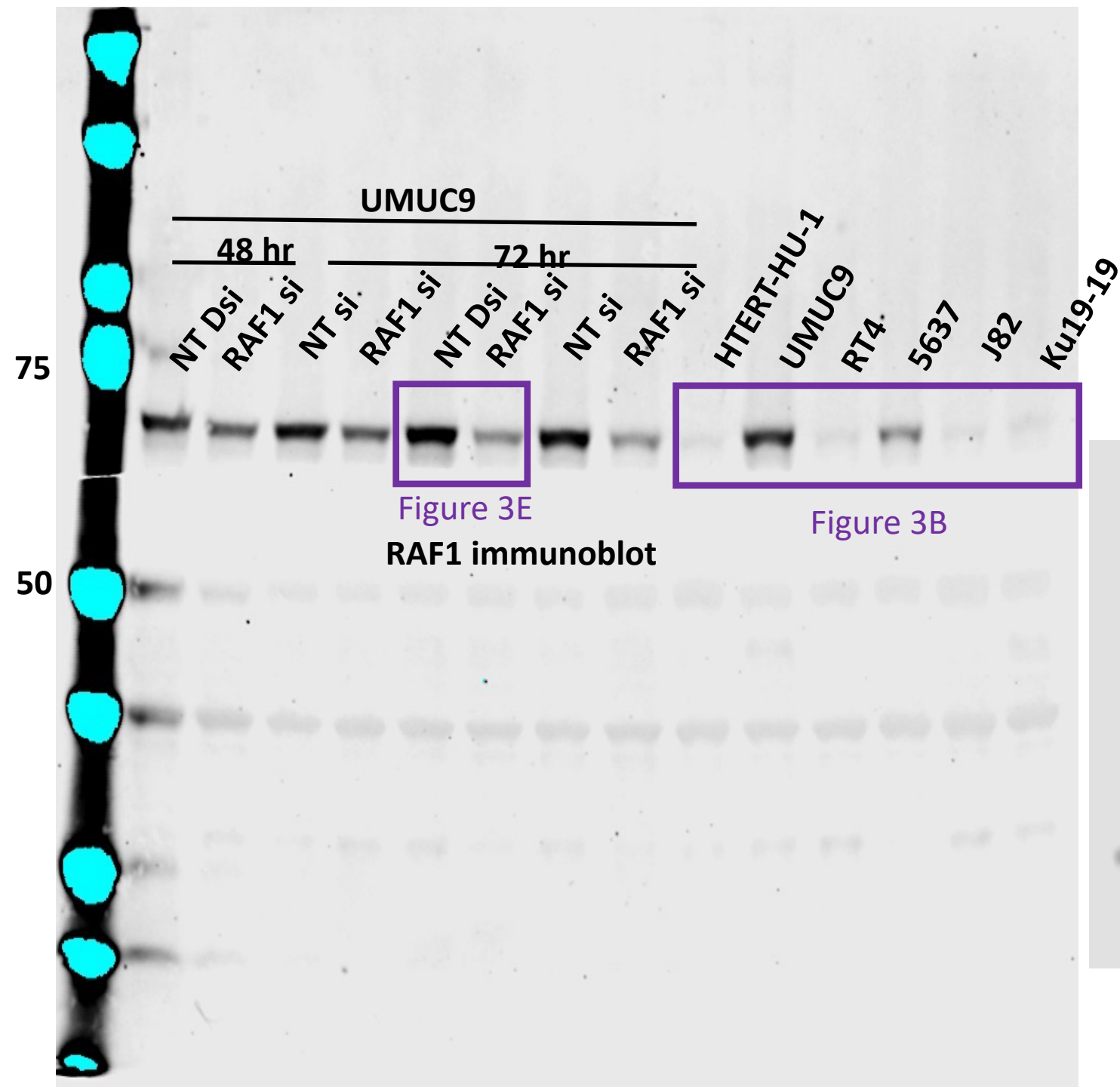


C)

Expression of MAPK pathway genes in luminal unstable (LumU) tumors from the TCGA (n=53)



Supplementary Figure 19: A majority of luminal–unstable (LumU) bladder tumors have at least one alteration in the mitogen–activated protein kinase (MAPK) pathway. (A) Twenty MAPK signaling pathway genes were included in the analysis. (B) Percentage of TCGA cases for each consensus subtype with a predicted functionally relevant alteration in at least one MAPK pathway gene (i.e., an activating mutation or gene amplification of a positive mediator of MAPK signaling such as *FGFR3*, or an inactivating mutation or gene deletion of a negative regulator such as *NF1*). More than 80% of luminal unstable (LumU) tumors have at least one alteration in a MAPK pathway gene. *RAF1* amplifications comprise approximately half of the MAPK pathway alterations in the LumU subtype whereas *FGFR1-3* alterations are most common in the luminal papillary (LumP) subtype. (C) Gene expression of MAPK pathway genes in LumU cases from the TCGA BLCA cohort.



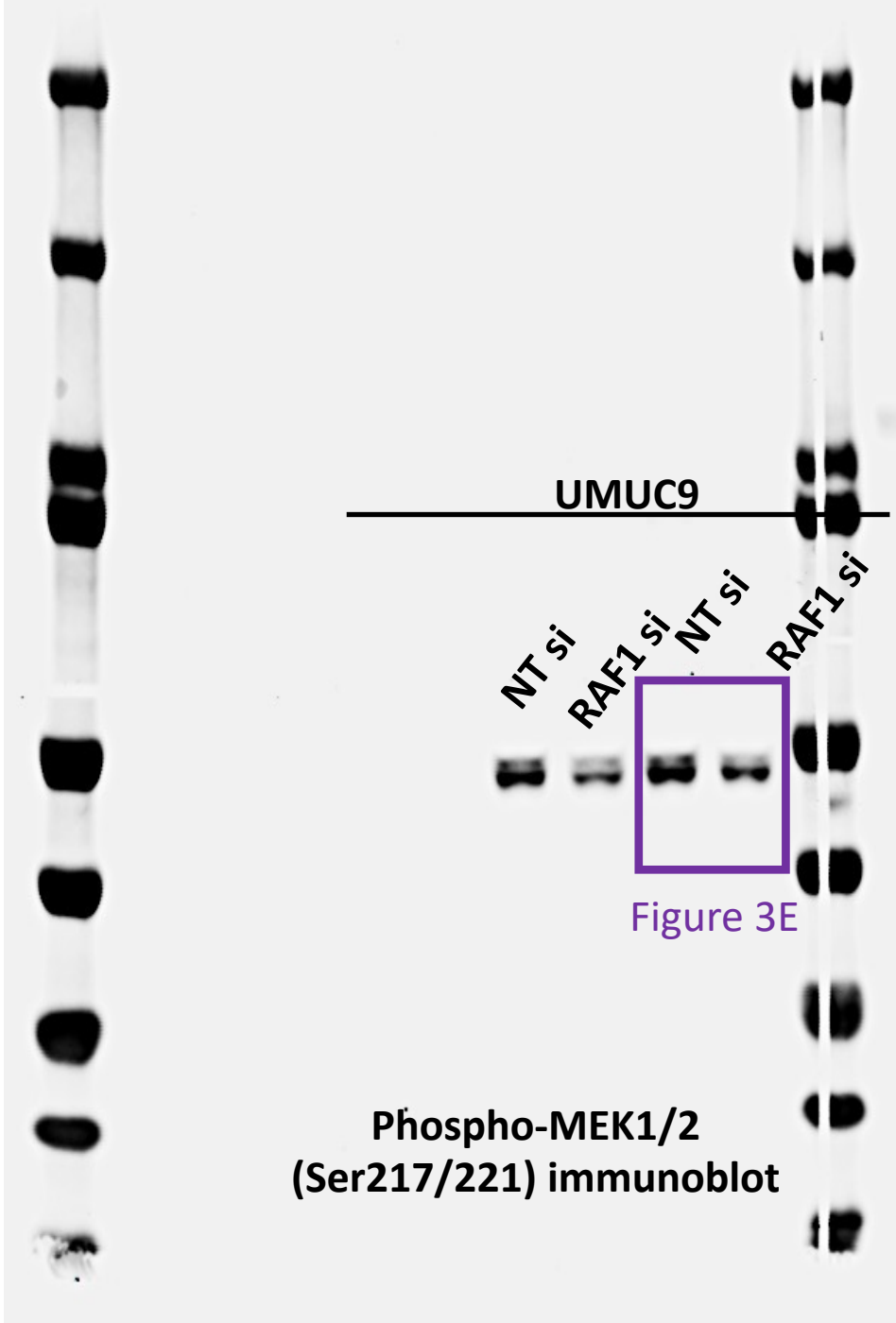


Figure 3E

UMUC9

NT si

RAF1 si

NT si

RAF1 si



Figure 3E

Phospho- Erk1/2 (Thr202/Tyr204) immunoblot



Figure 3E

UMUC9
NT si RAF1 si NT si RAF1 si

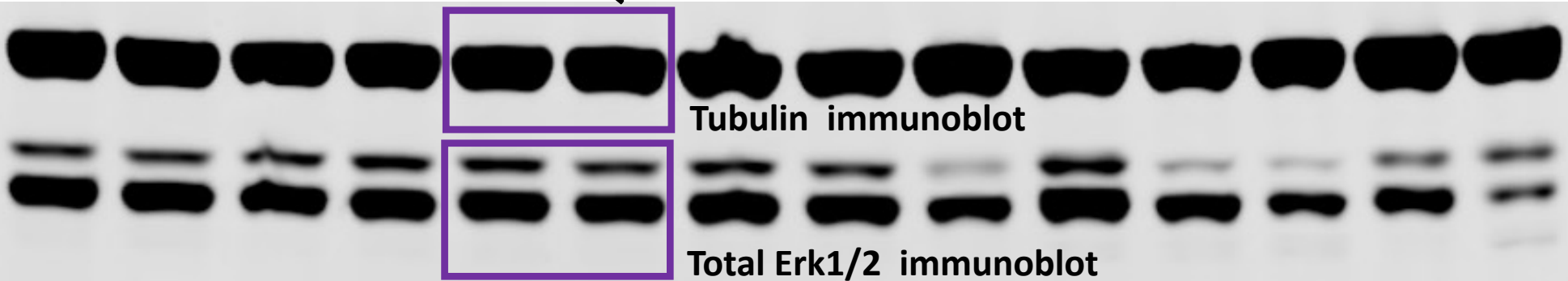
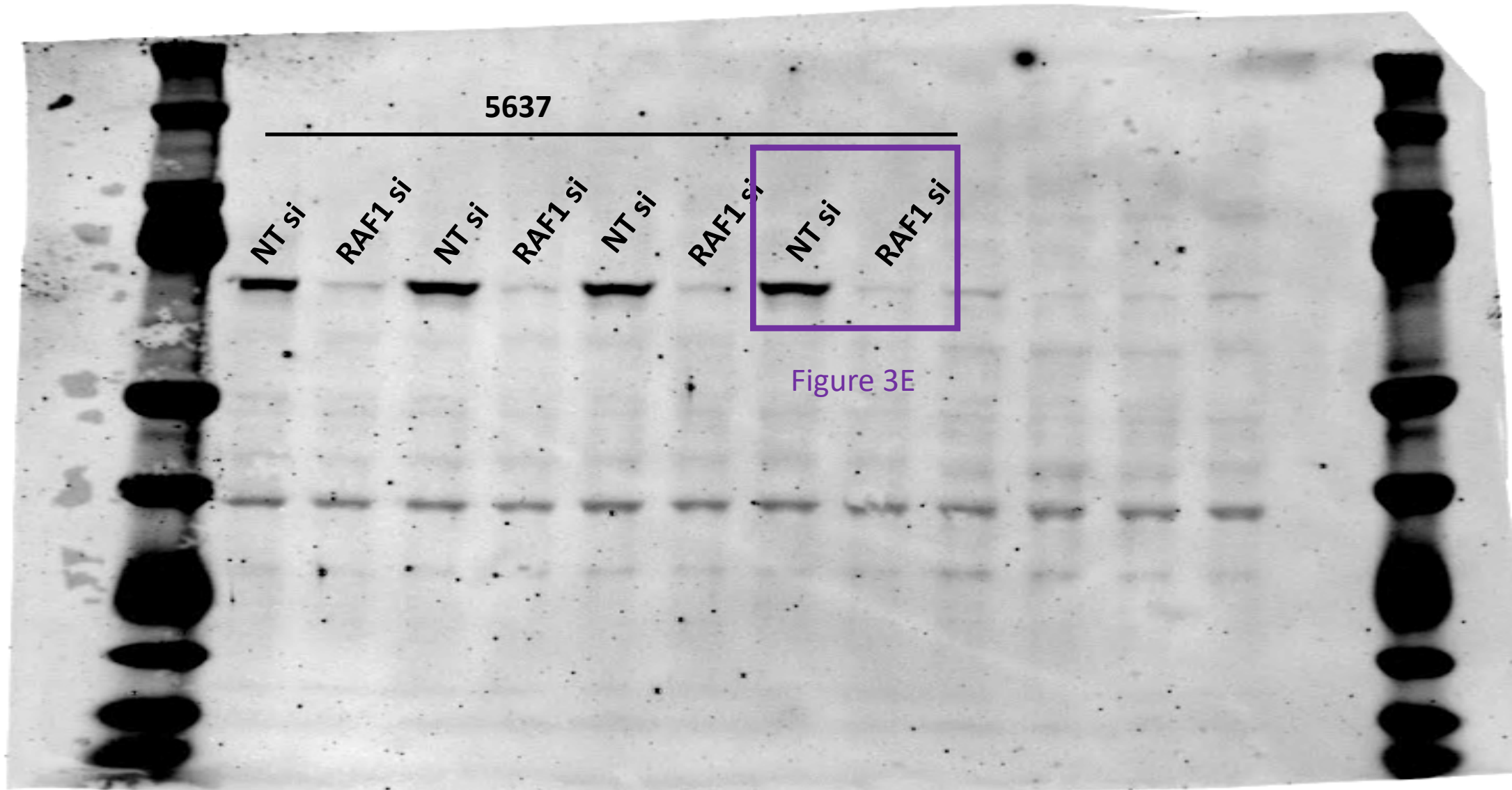


Figure 3E

Figure 3E



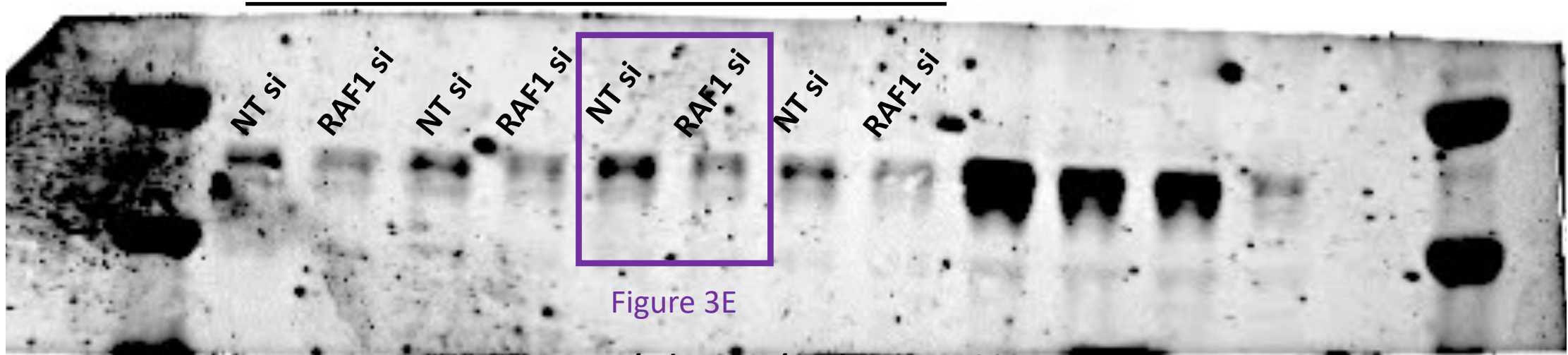
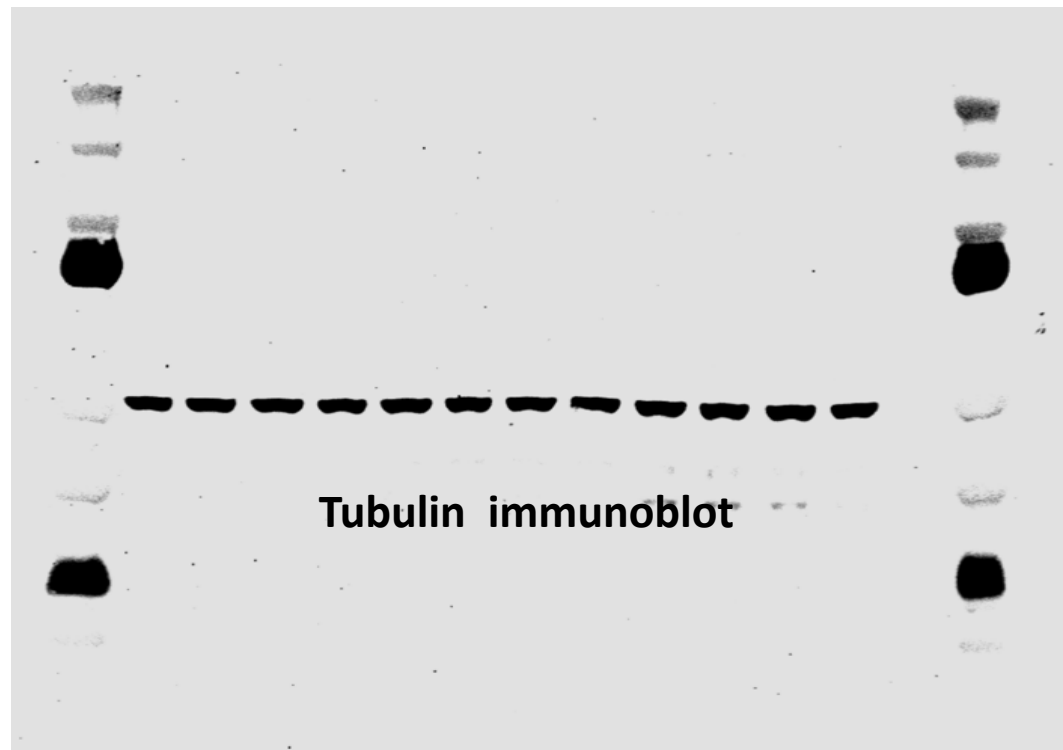


Figure 3E

Phospho-MEK1/2 (Ser217/221) immunoblot



Tubulin immunoblot

Figure 3E

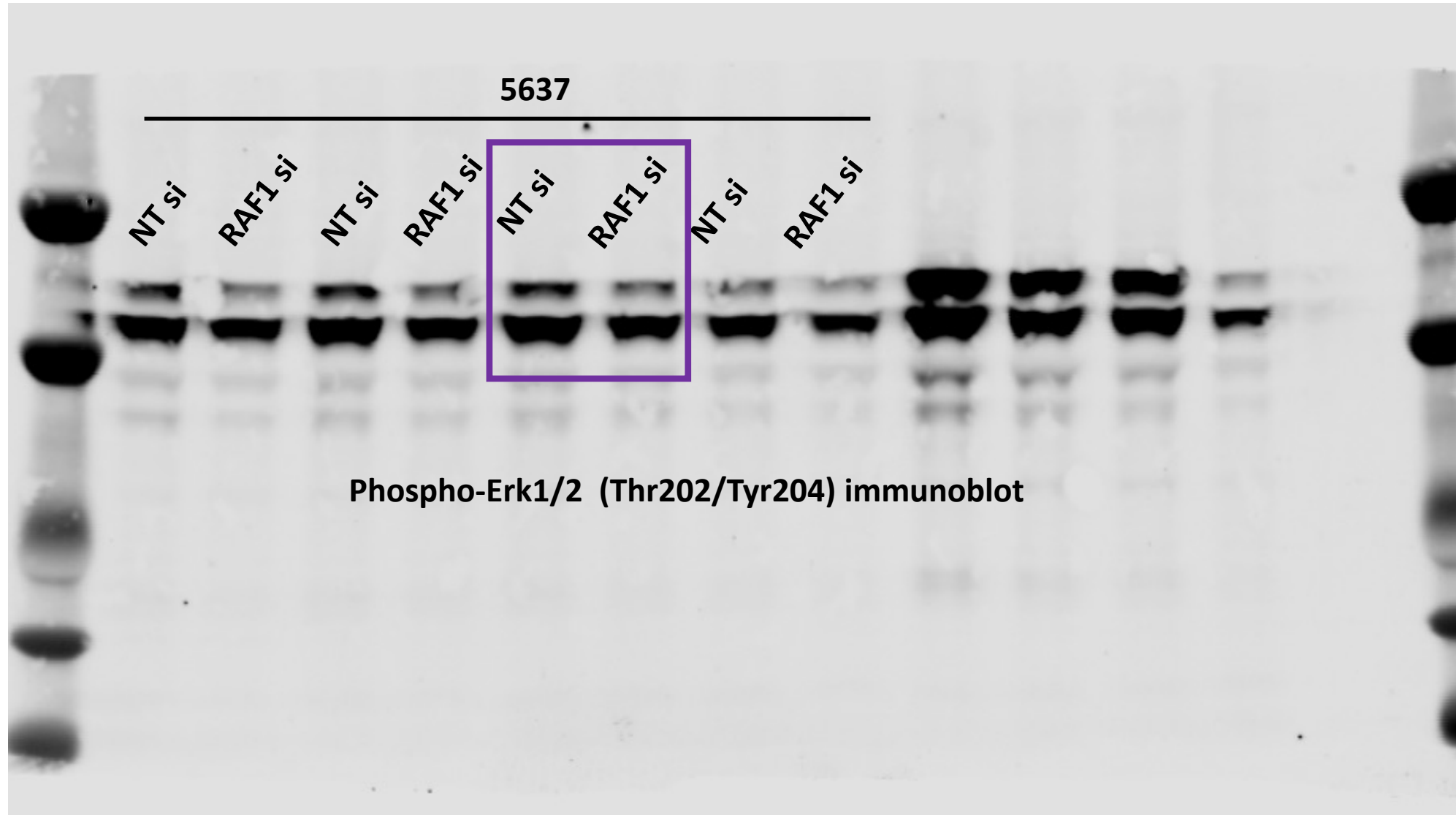
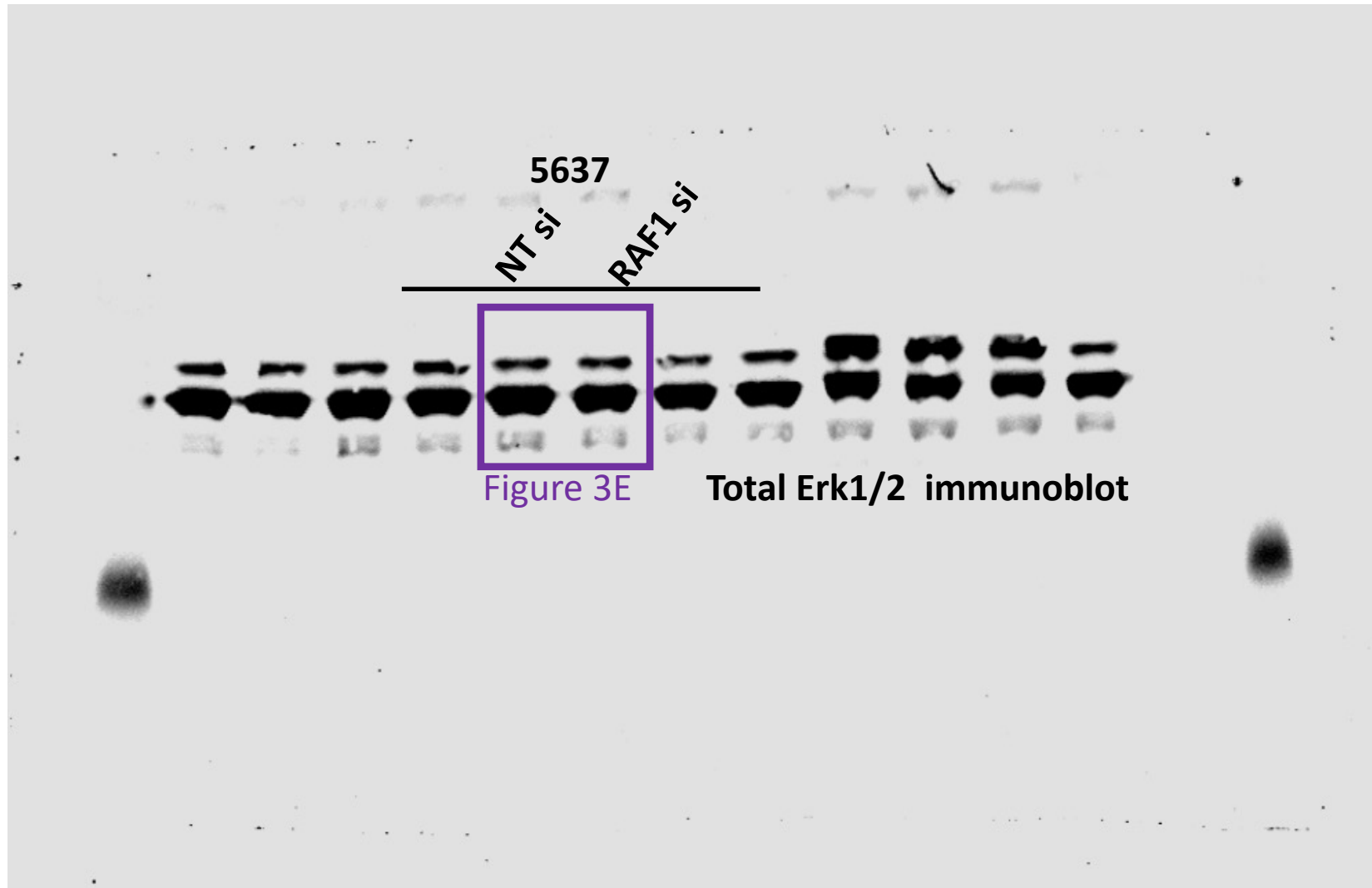
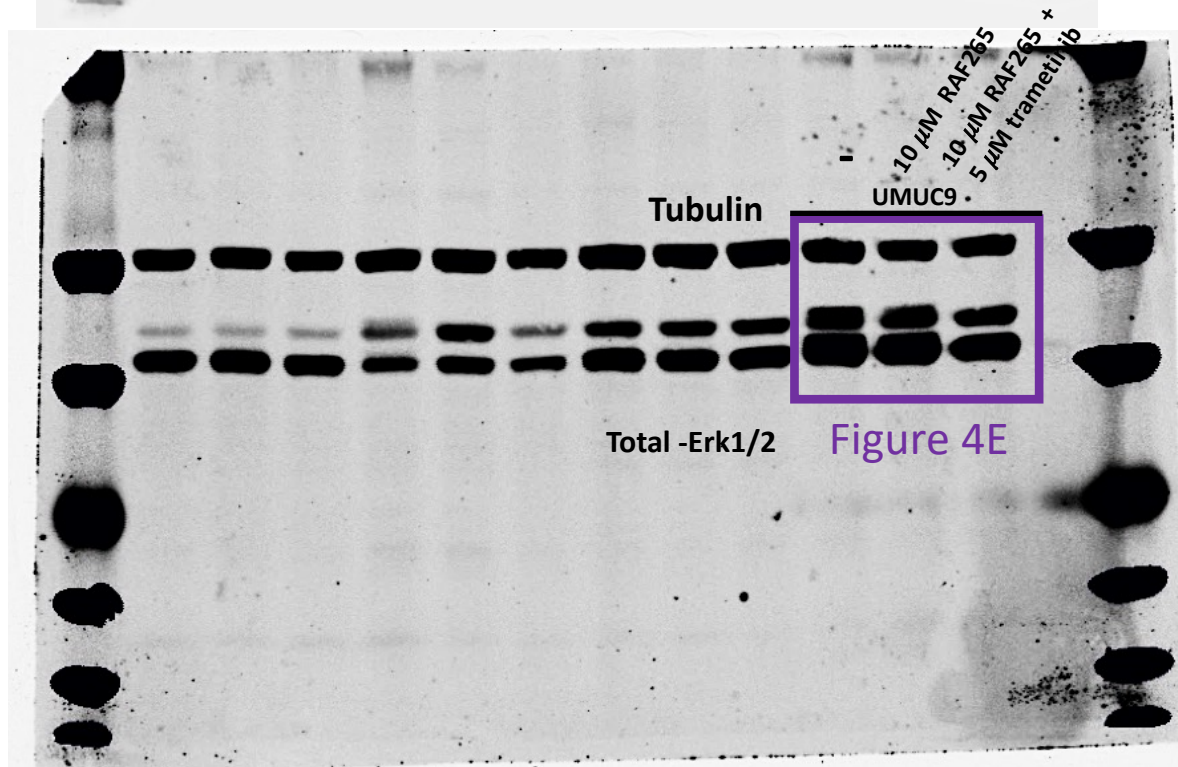
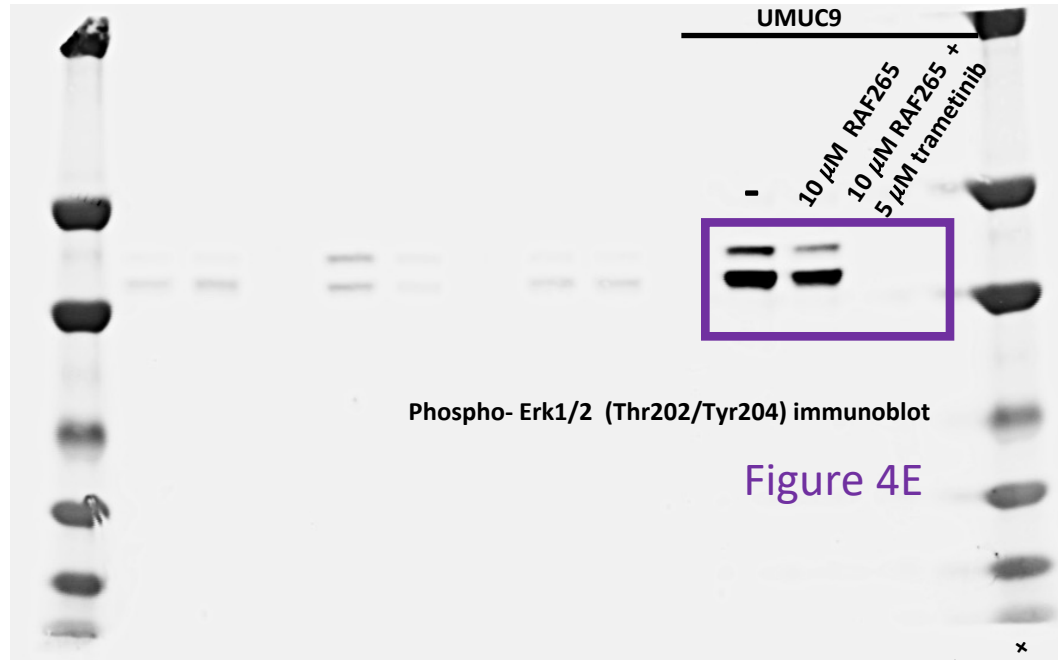


Figure 3E





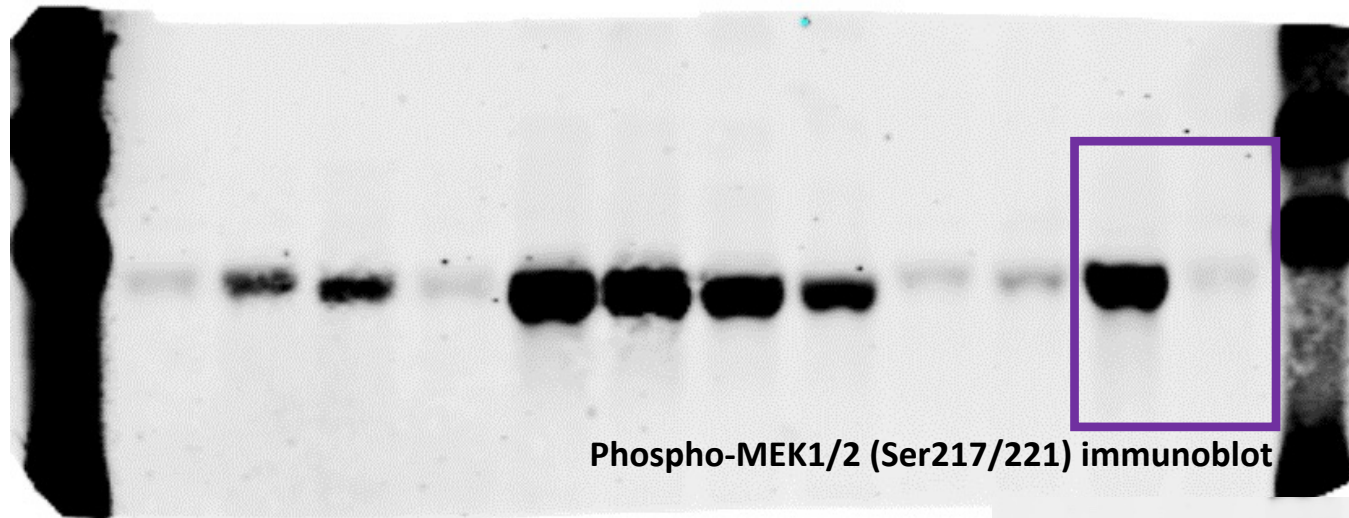


Figure 7C

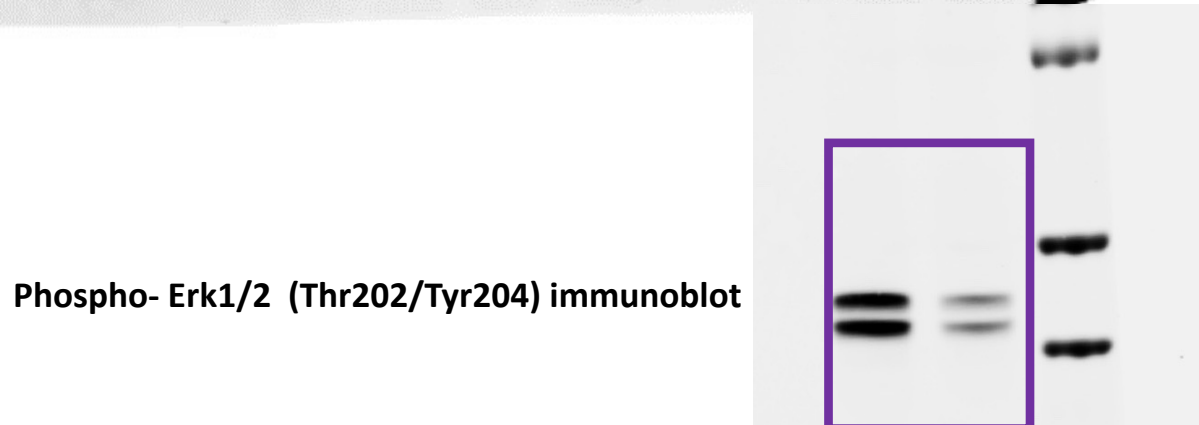
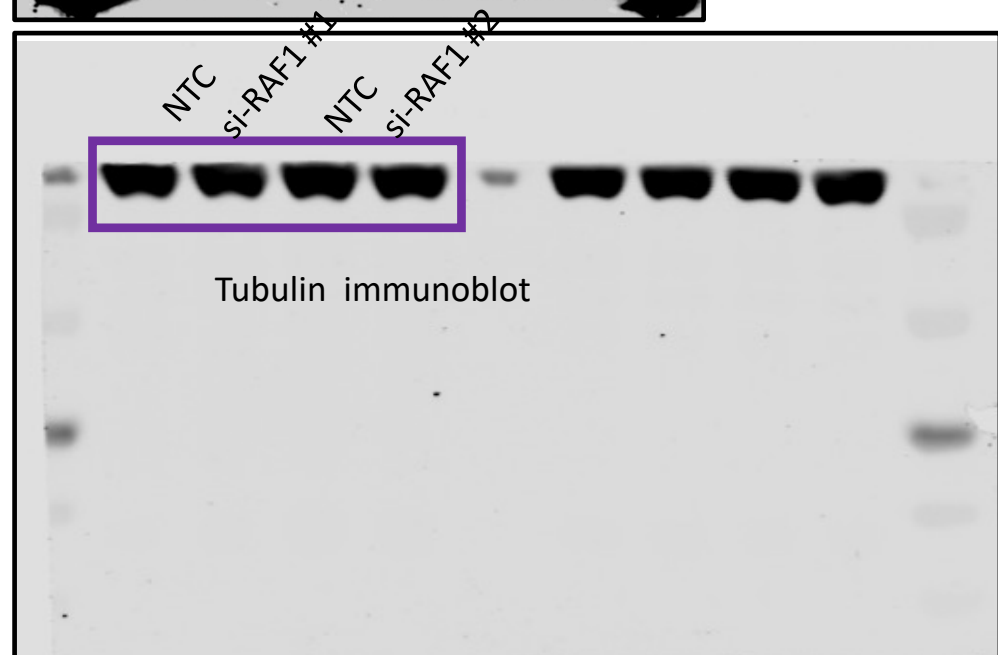
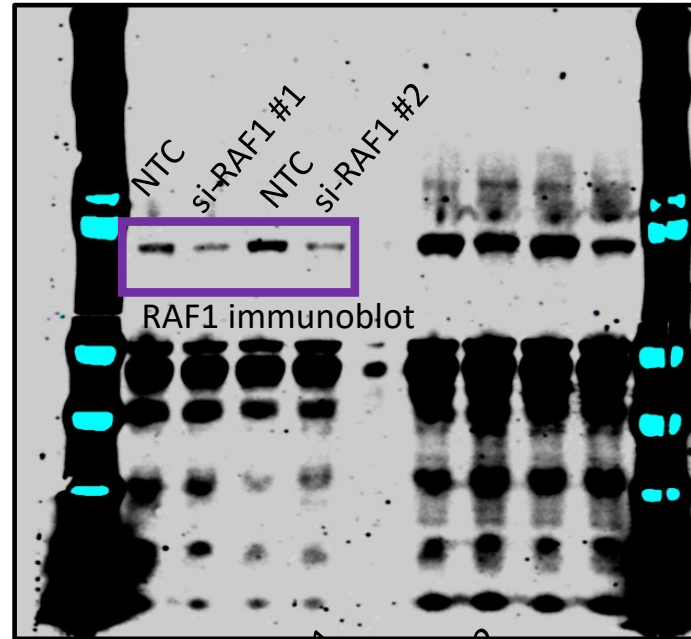
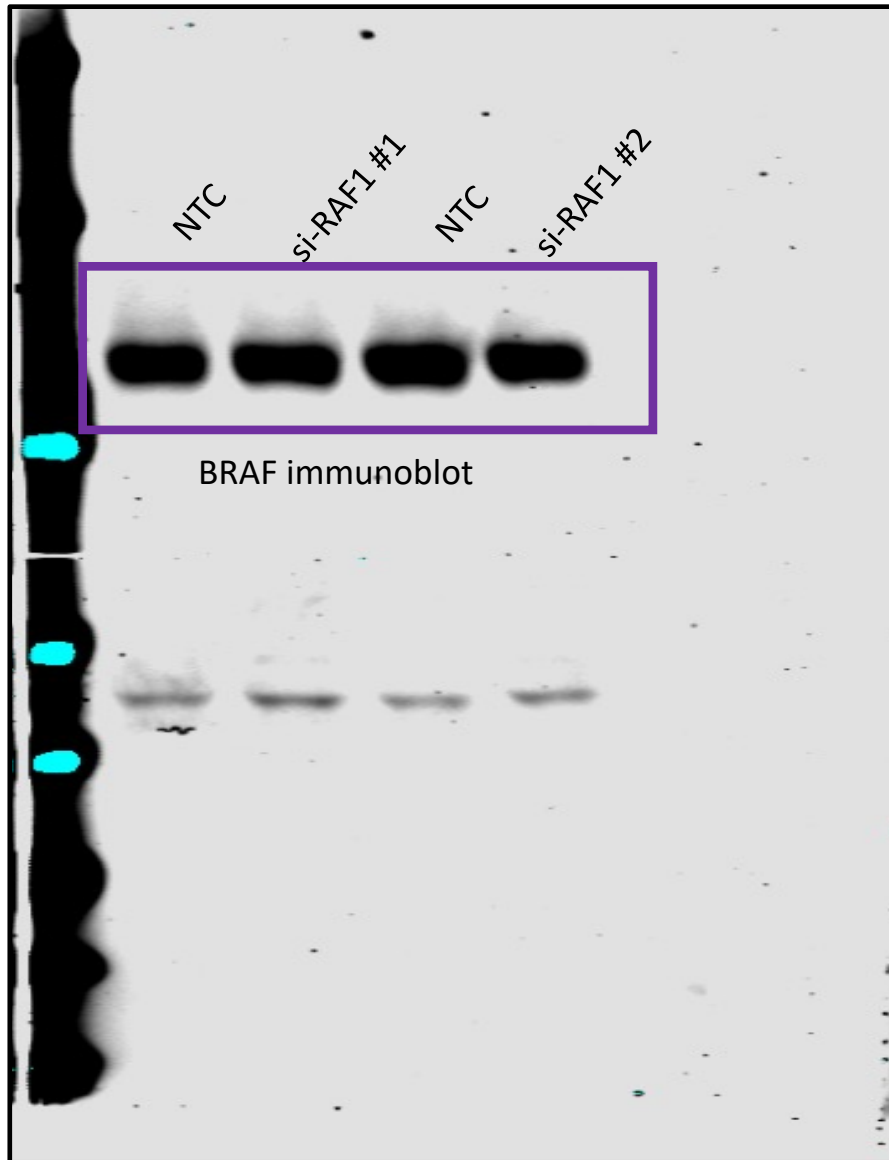


Figure 7C

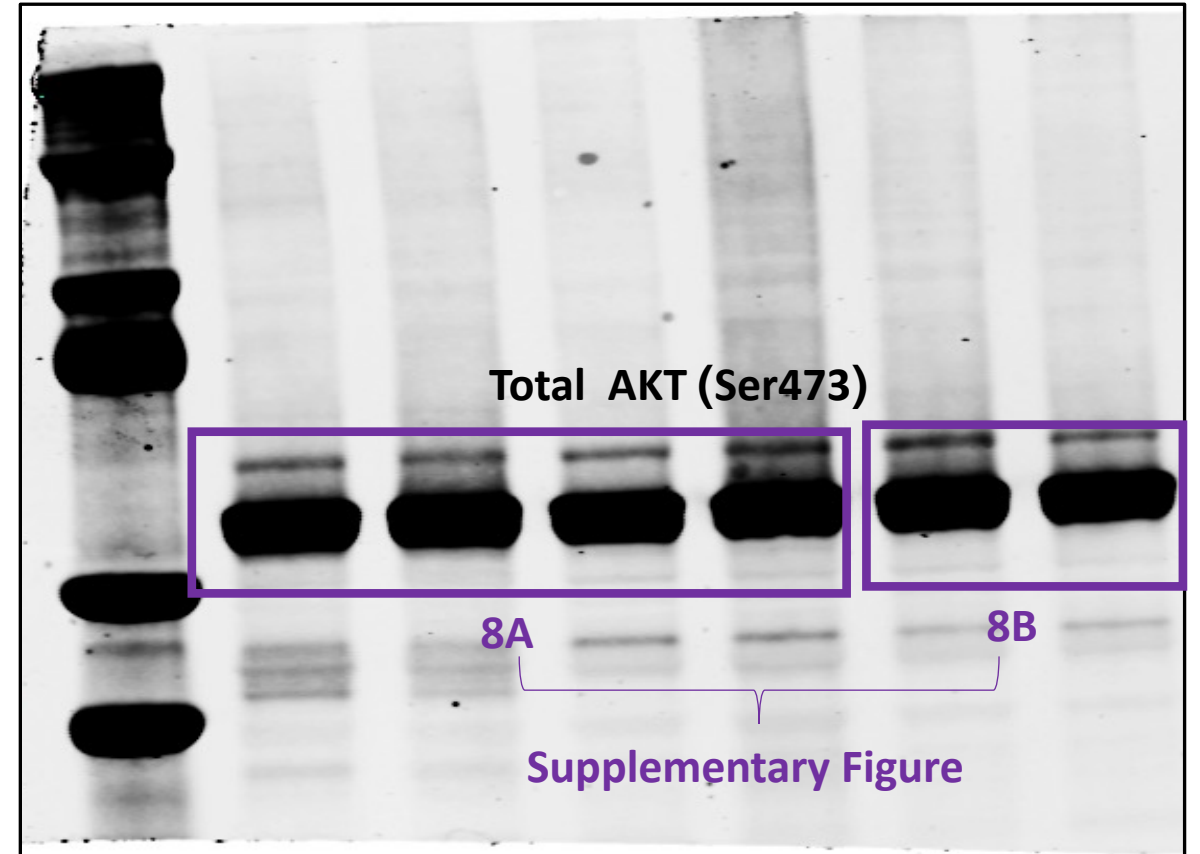
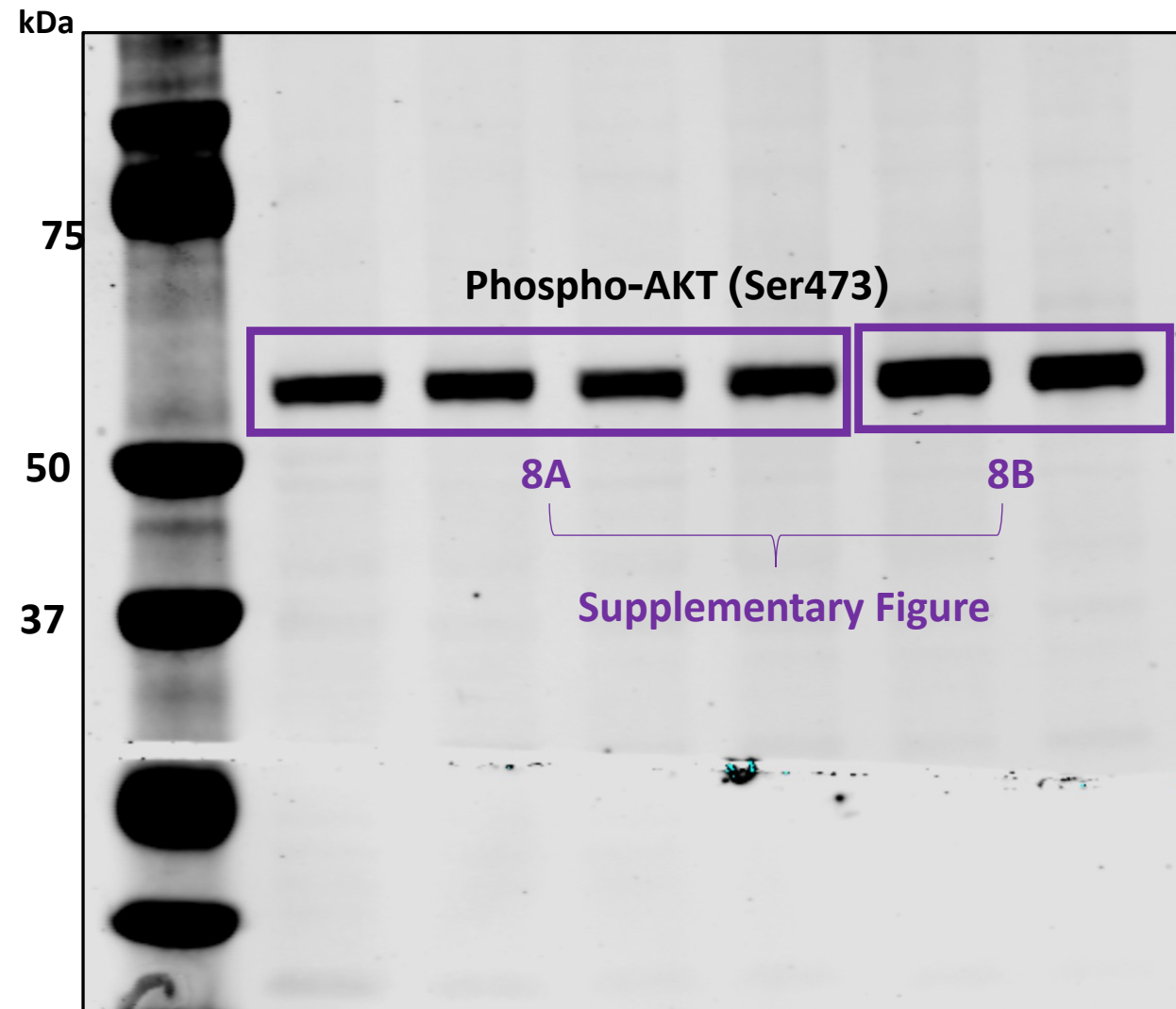


Figure 7C

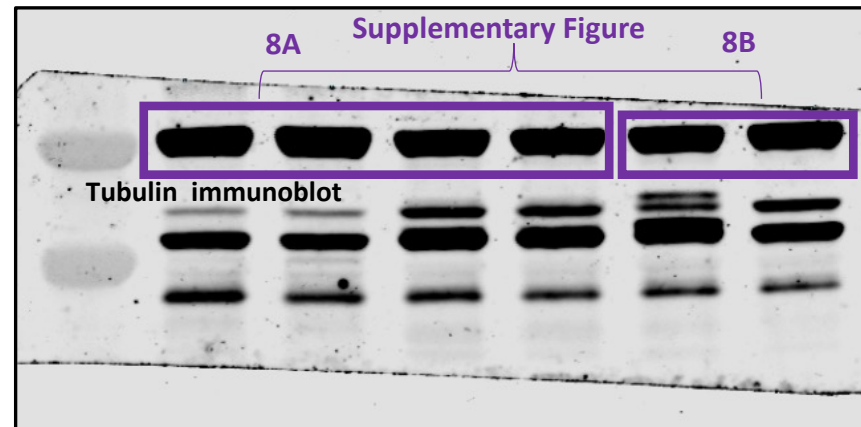
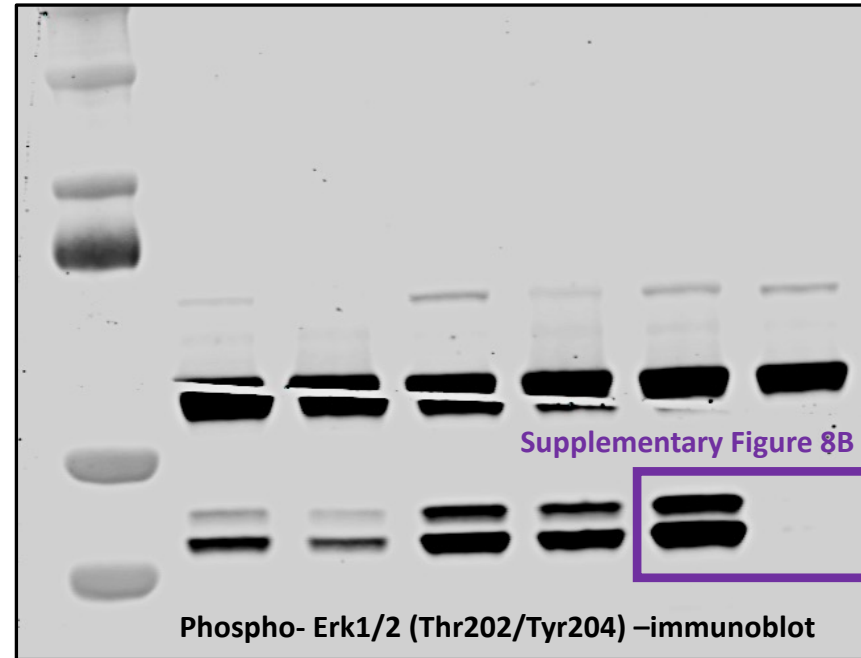
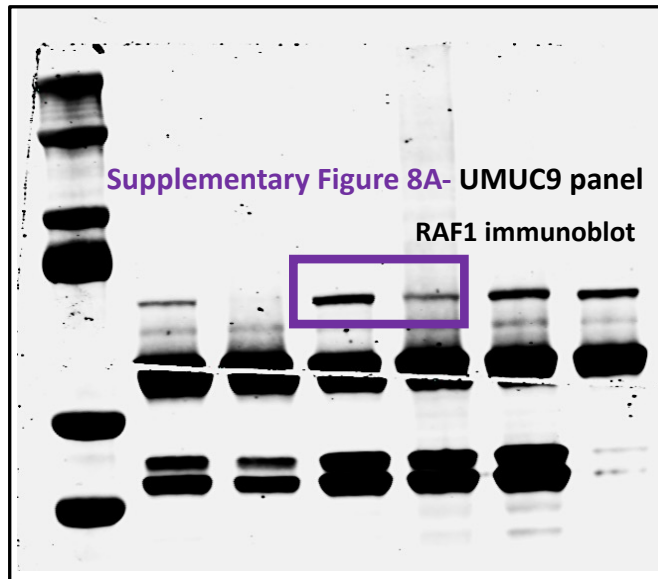
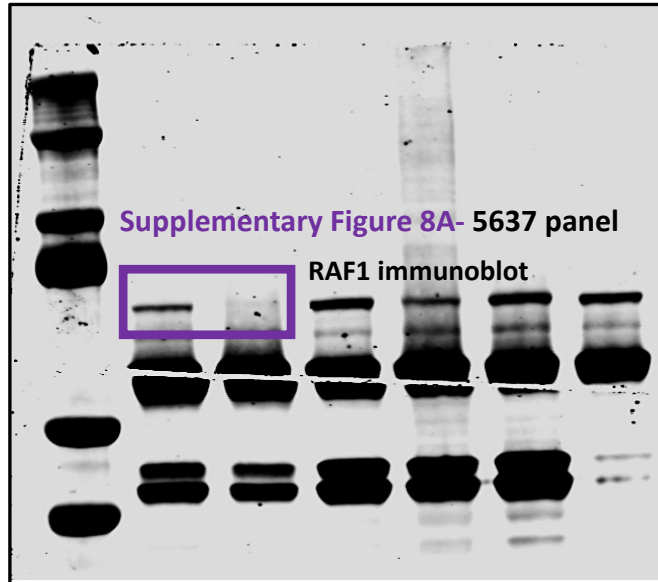
Supplementary Figure 7A



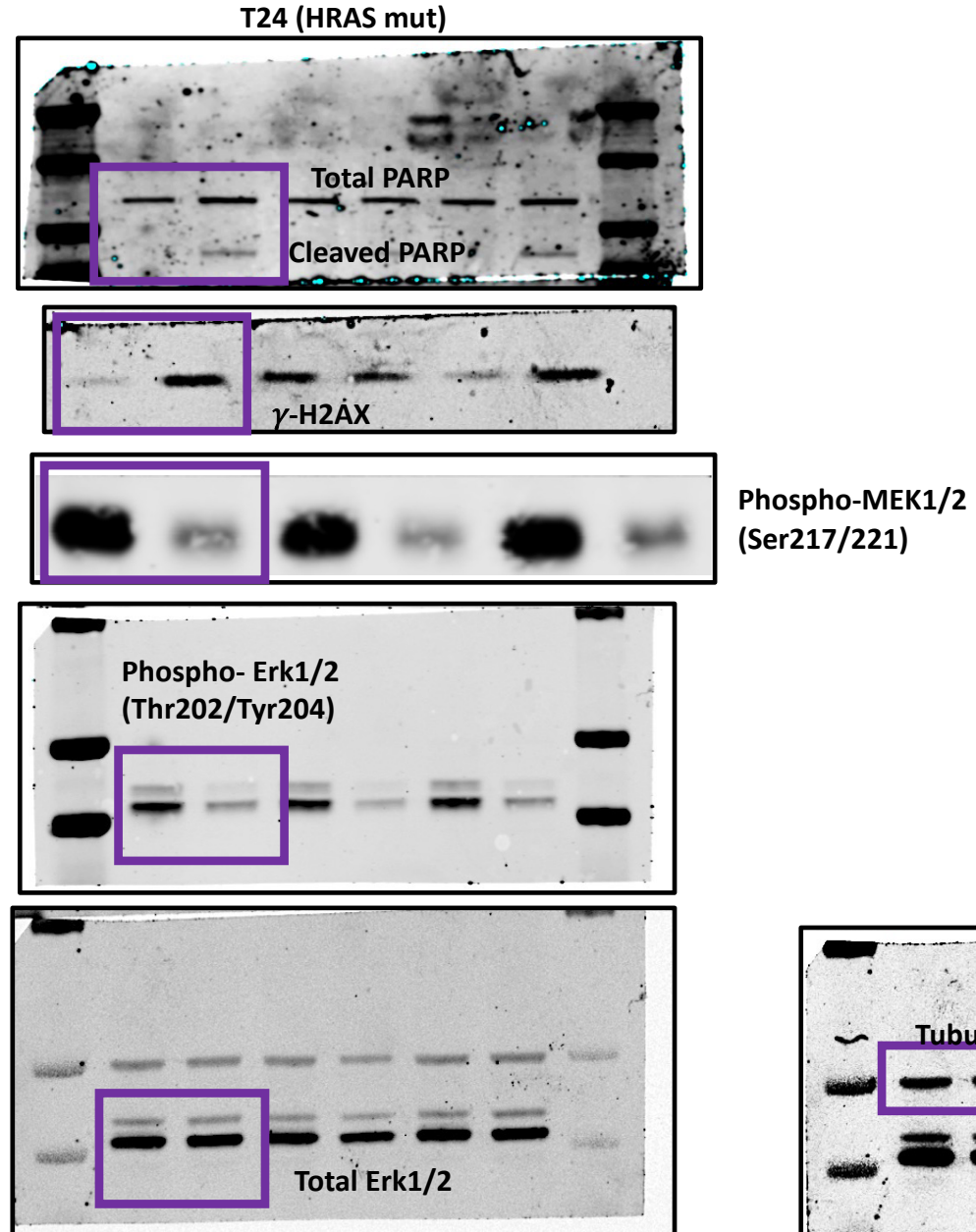
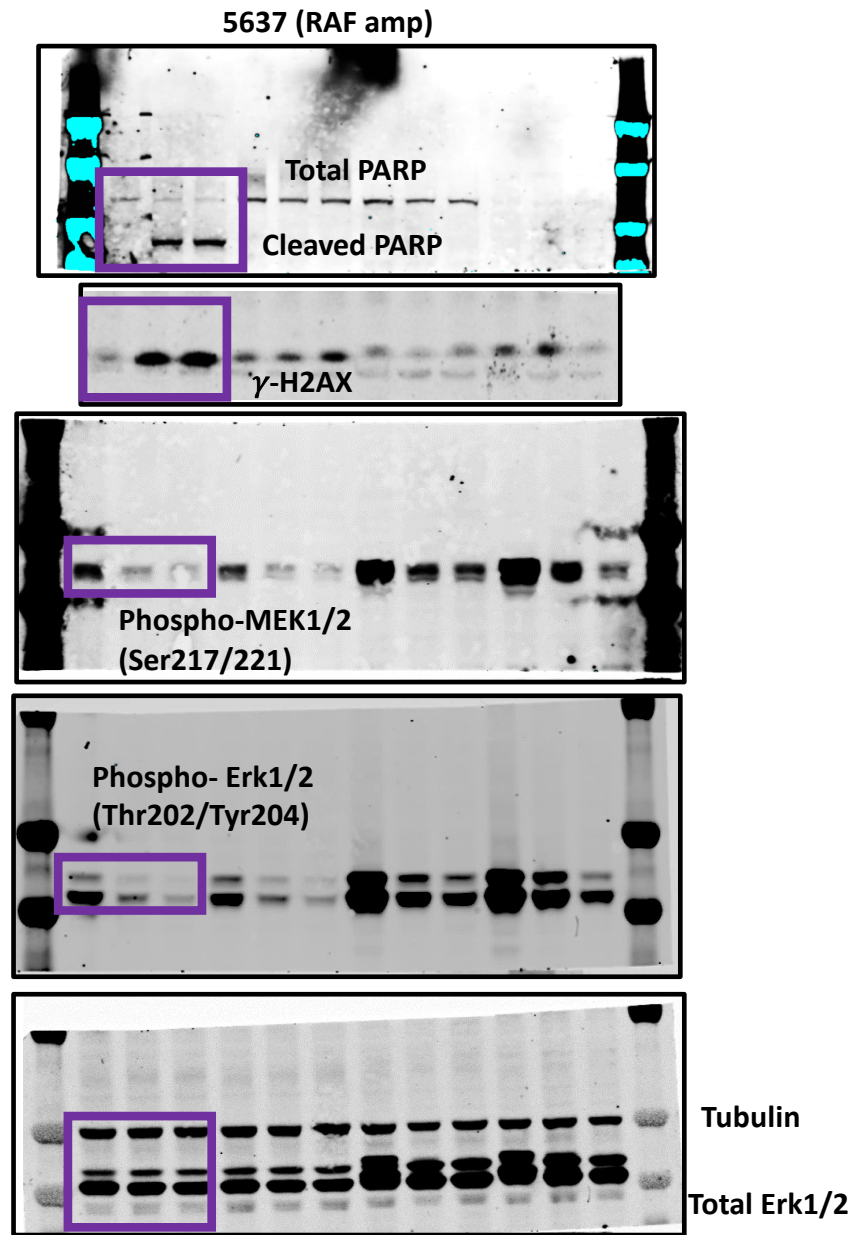
Supplementary Figure 8A & B

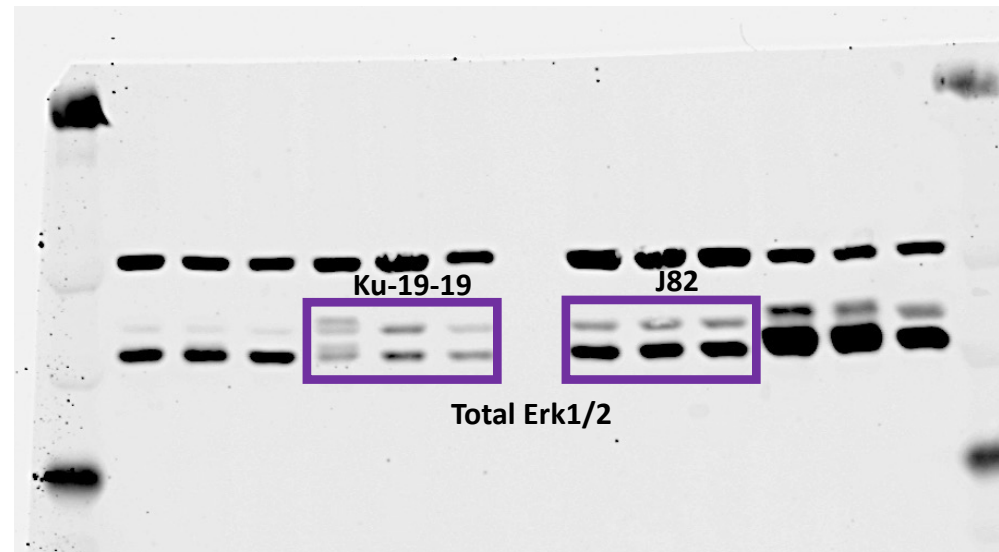
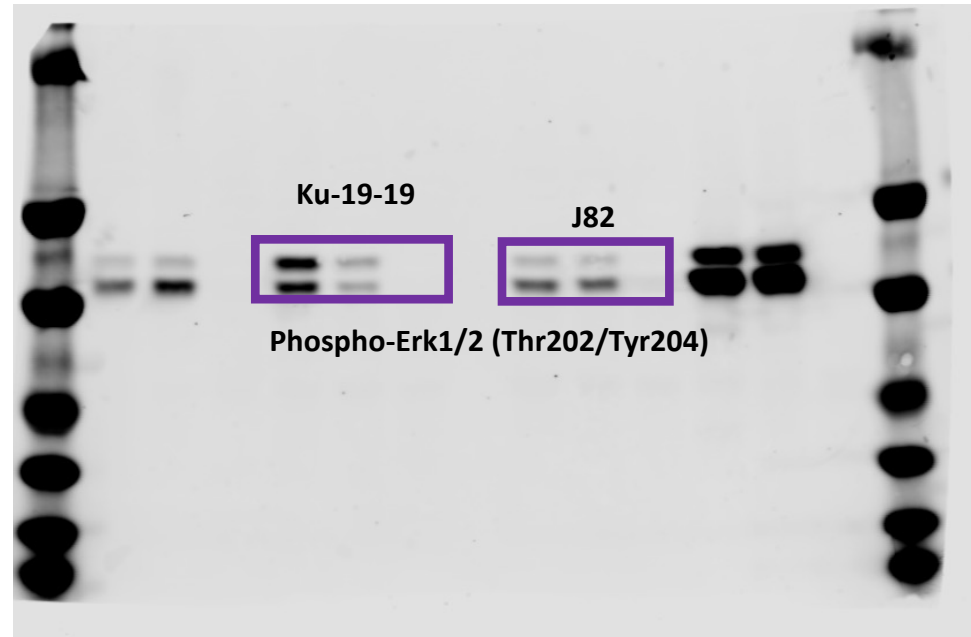


Supplementary Figure 8A & B



Supplementary Figure 14B





Supplementary Figure 16C

